FATIGUE AND WEAR OF STEEL EYEBARS FROM HISTORIC RAILROAD TRUSS BRIDGES

A Thesis

by

CARLOS ALBERTO BROWN

Submitted to the Office of Graduate and Professional Studies of
Texas A&M University
in partial fulfillment of the requirements for the degree of

MASTER OF SCIENCE

Chair of Committee,	Peter Keating
Committee Members,	Gary Fry
	Vikram Kinra
Head of Department,	Robin Autenrieth

May 2017

Major Subject: Civil Engineering

ABSTRACT

Fatigue of steel is a major cause of mechanical failure and as such is very important to the safe design of railroad bridges. Fatigue phenomena are governed by the creation and growth of cracks, which can propagate through the material under stress until the material fails from fracture. Since these cracks take time to form and grow, cyclic loading is the main driver of fatigue in steel.

Two historic steel-truss railroad bridges were dismantled and several joints were extracted intact from each bridge. Historic railroad bridges built around the turn of the 19th century were mostly not designed for fatigue, so it has become necessary to study these bridges to understand their fatigue behavior.

Additionally, many in-service bridges in the United States are very old, are approaching the end of their useful service lives, and do not have accurate as-built information readily available. Much research has been done to develop and evaluate experimental methods to evaluate the structural health of bridges in situ, however these often rely heavily on certain assumptions that may or may not hold. Often historic bridge behavior is a surprise to engineers and gives unexpected results. Accurate knowledge of material properties is of utmost importance in understanding how these bridges will behave. Therefore, several aspects of the structural form are investigated including the wear of the components during service life, material test results, and fatigue behavior of the eyebars.

ACKNOWLEDGEMENTS

I would like to thank my committee (Dr. Keating, Dr. Fry, and Dr. Kinra) for their guidance and support throughout the course of this research.

Thanks also go to Matt, Ramiro, and Charlie for their lab expertise and the many laughs to lighten the mood during research hours.

I would like to thank the Association of American Railroads for providing the financial support for this project.

Finally, thanks to my mother, father and RCB for their encouragement and love. I am very grateful for your support.

CONTRIBUTORS AND FUNDING SOURCES

Contributors

This work was supported by a thesis committee consisting of Professor Peter Keating [advisor] and Professor Gary Fry of the Department of Civil Engineering and Professor Vikram Kinra of the Department of Aerospace Engineering.

All work conducted for the thesis was completed by the student independently.

Funding Sources

Graduate study was supported by research funding from the Association of American Railroads.

NOMENCLATURE

ksi	Kips per in^2
EDF	Empirical Distribution Function
ANOVA	Analysis of Variance Test
AD	Anderson Darling Test
S-N	Stress Range vs Cycles to Failure

TABLE OF CONTENTS

Page

LIST OF FIGURES

Page

LIST OF TABLES

Page

CHAPTER I

INTRODUCTION

The scheduled replacement of two historic railroad bridges provided the opportunity to experimentally examine steel eyebar members. During demolition of the bridges, numerous joints with connecting members were preserved. The data gathered from the components of these joints, along with original drawings and documentation, are used as the basis of the findings for this report. The goal of this research study is to quantify and characterize fatigue and material behavior of steel truss bridge eyebars of turn of these 19th century railroad bridges, including the interaction of fretting wear with fatigue life of the eyebar.

Destructive testing was to be used as the most accurate method of obtaining data. The material properties desired were the tensile yield strength and fatigue life as prescribed by the S-N curve. Additionally, fretting wear measurements were taken on the eyebar pin holes. The interplay of these variables was investigated after the experiments in order to ascertain if there are any significant relationships between the examined variables. Specifically, the behavior of the fretting wear of components was mathematically characterized and correlated with other material properties. The main goal of the study is not only to obtain representative material data for historic period bridges, but to quantify the fatigue behavior of the eyebars, in particular the fatigue threshold or constant amplitude fatigue limit, in order to allow for better fatigue assessment of in service bridges of similar age and configuration.

CHAPTER II

BACKGROUND

2.1 Background

The objective of the research reported herein is to experimentally characterize the material and fatigue properties of different steel eyebar materials taken from the Burlington Bridge in Iowa and an unnamed bridge in Oregon of similar layout and design. These bridges are known to have been constructed around the turn of the 19th century (1893 for the Burlington bridge), and their subsequent demolition for replacement has offered a unique opportunity to study some of their material properties.

Many in-service bridges in the United States are very old and are approaching the end of their useful service lives. Much research has been done to develop experimental methods to evaluate the structural health of bridges in situ, however these often rely heavily on certain assumptions that may or may not hold. Modern manufacturing techniques have not only improved the material properties of steel such as the tensile yield and ultimate strengths, but they have also reduced the variance in expected properties. This study investigated the assumption that pre-standardization materials were highly variable in their properties.

Low variability in material properties is essential to proper design. Without proper understanding of this variability, structural failures may occur. However, lessons can be learned from these infrequent incidents. Probably the most notable in recent history is the collapse of the Silver Bridge in Gallipolis, Ohio in 1967. The bridge was

constructed in 1928 as an eyebar chain suspension bridge (Nishanian and Frank 1972). Causes contributing to the failure were determined to be fatigue, stress corrosion cracking and lack of redundancy in the eyebar suspension chain that supported the bridge deck.

The Burlington Bridge is a Pratt Truss Steel Bridge constructed in 1893 in Burlington, Iowa for the Chicago, Burlington, and Quincy Railroad. The chief engineer of the Burlington Bridge project was George S. Morison and contractor was the New Jersey Steel and Iron Company out of Trenton New Jersey (Morison 1893). The bridge stayed in service until late 2009 when work began to replace it with a new swing span and superstructure. The Burlington Bridge supported two tracks which replaced a single track structure constructed in 1867. Figure 2-1 on the next page shows the layout of the bridge superstructure as it was designed in 1893.

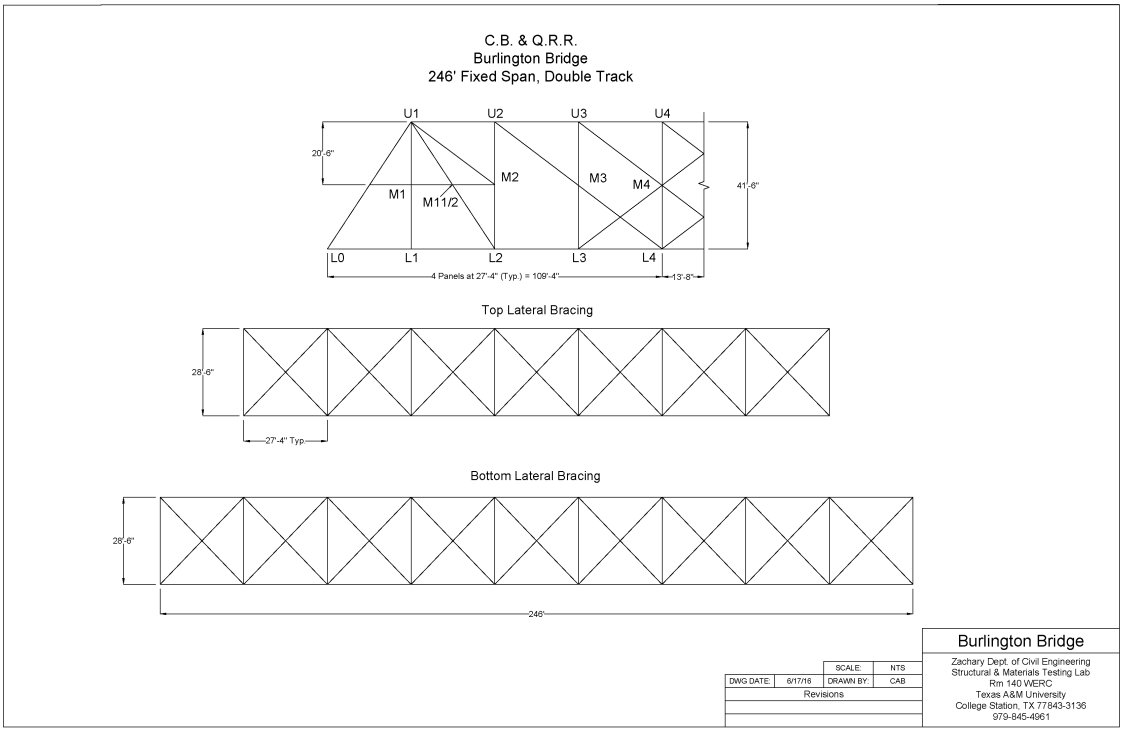

Figure 2-1 – Burlington Bridge Superstructure

Table 2-1 provides the cross sectional dimensions of the eyebars. It is important to note that multiple eyebar sections were used in a given eyebar member and varied between four and eight in number.

Table 2-1 – Eyebar Connectivity

Joint i	Joint j	Size (WxT)	# Bars	Pin Diam.
L2	L3	7"x1""	8	6"
L2	L3	7"x2"	8	6"
L3	L4	7"x2 1/4"	8	6"
L4	L4	7"x1"	4	6"
L4	L4	7"x2"	4	6"
L4	L4	7"x2 1/8"	4	6"
U1	M1	7"x1 1/4"	8	6"
U1	M1 1/2	7"x1 3/4"	8	6"
U1	M2	7"x1 3/4"	8	6"
U2	M3	7"x1 3/8"	8	6"
U3	M4	7"x1"	8	6"
M2	L3	7"x1 3/4"	8	6"
M3	L4	7"x1 3/8"	8	6"
M4	L4	7"x1"	8	6"
M1 1/2	L2	7"x1 3/4"	8	6"
M1	L1	7"x1 1/4"	8	6"
U4	M4	4"x1"	8	6" & 4"
M4	L3	4"x1"	8	6"

Steel eyebars formed the main body of the tensile resisting members of the truss, and were manufactured using the open hearth process. The eyebars were first formed by forging and upsetting the heads into the desired shape (Morison 1893). Pin holes were then bored into the heads. The bars were subsequently annealed in an annealing furnace and allowed to cool slowly. The specification written by Morison does not specify the exact temperature of annealing. A review of period literature suggests that annealing was controlled by color of the glowing metal rather than exact temperature readings and the color of annealing was not specified. After the bar was cooled and inspected, a single

coat of Cleveland Iron Clad paint, purple brand, was applied to the bar with boiled linseed oil and the eyebar was shipped off to the bridge site.

The second bridge in this study is the Oregon Bridge. While it is known that the bridge is from Oregon and had a similar configuration to the Burlington Bridge, no other information about this bridge is available from the railroad.

2.2 Literature Review

2.2.1 S-N Curves

Fatigue life prediction of structural members under constant amplitude loading can be achieved with stress range versus number of cycles to failure or S-N curves as first recognized by August Wöhler in 1867 (Schütz 1996). Interesting to the current study, fatigue failures were "byproducts of the industrial revolution," which combined with westward American expansion drove the construction of many railroads, and consequently railroad bridges.

The earliest study that Wöhler performed was on fatigue of railcar axles. From these investigations, he constructed the ubiquitous S-N curve, sometimes referred to as the Wöhler curve. The S-N curve shows the relationship between the applied stress range (constant amplitude) and the resulting fatigue life in N cycles to failure at the given amplitude. Fatigue cracks are created (nucleated) by the application of cyclic stresses, characterized here by stress range, which continue to grow the crack until fracture occurs at N cycles. Below, Figure 2-2 shows a typical S-N curve for two different materials. Ferrous materials like steel usually exhibit a fatigue threshold, sometimes called the endurance limit or fatigue limit, under which theoretical infinite

fatigue life can be obtained. Other materials with different molecular structure such as aluminum do not show this same behavior and will eventually fail at any cyclic stress range applied.

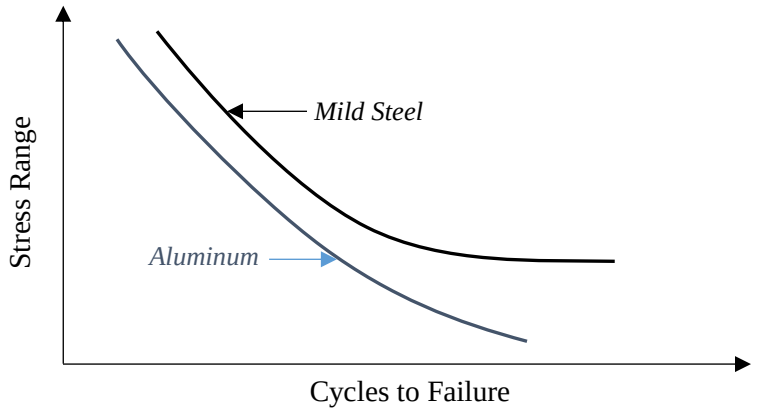

Figure 2-2 – Typical S-N Curve

Figure 2-3 shows the relationship between the fatigue threshold and crack growth. Stresses ranges below the threshold do not nucleate or propagate cracks, however all stress ranges above the threshold do.

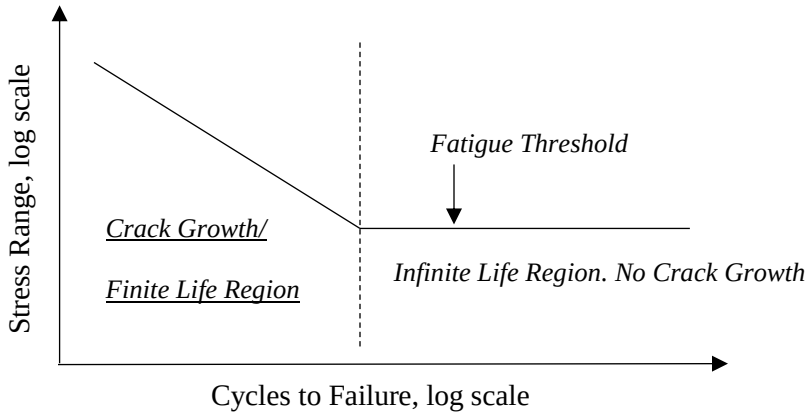

Figure 2-3 – Crack Growth S-N Curve

The S-N curve holds true only for constant amplitude loading. Laboratory tests that produce an S-N curve are time consuming and expensive as well. A drawback of the S-N curve method is that it is impractical to create a useful set of curves that can cover many different combinations of mean stress, alternating stress, and stress ratio (R). Overall, the S-N test has its usefulness in showing how a material behaves on a macro scale and represents the backbone of fatigue analysis of metals. The S-N curve is employed in the current study. A main goal of the present study is to identify the fatigue limit for the class of steels used in the construction of these two bridges.

The S-N curve has two different regimes governing which depend on the applied stress ranges. High Cycle Fatigue (HCF) is in the elastic range with stresses below the yield stress of the material whereas Low Cycle Fatigue, governed by the Coffin-Manson relation, produces plastic deformations due to the high stress, therefore the behavior is different (Schijve, Schijve et al. 2001). The Coffin-Manson relation is as follows

$$\frac{\Delta\varepsilon_p}{2} = \varepsilon'(2N)^c \quad (1)$$

where $\frac{\Delta\varepsilon_p}{2}$ = plastic strain amplitude, ε' = fatigue ductility coefficient, $2N$ = number of strain reversals to failure, and c = fatigue ductility exponent. Strain is usually found to be a better predictor than stress in the Low Cycle regime. The reason for this is that due to the plastic deformation that can occur, with the accompanying change in true stress, strain becomes a more consistent and convenient tool for prediction than stress. High Cycle fatigue can be modeled by the Basquin equation (Basquin 1910),

$$N * \sigma_a^p = C \quad (2)$$

where N = cycles to failure, p and C are empirical constants, and σ_a= stress amplitude

Basquin built off of Wöhler's earlier pioneering work to build a mathematical model that is still in use today as a descriptor of the S-N curve. Taking the log of the Basquin equation produces the following straight line equation (Eq. 3). The empirical constants can readily be deduced from the plot of experimental data using the slope of the line and Y intercept.

$$\log(N) + p * \log(\sigma_a) = \log(C) \quad (3)$$

Here the Y intercept of the straight line equation is $\log(C)$ and p is the inverse of the slope of the straight line. Using the fitted constants, the equation can be used to estimate the number of cycles until failure at a given stress level. It has been noted that scatter is reduced in the low cycle regime because crack nucleation begins early on in the lifecycle of the material, and therefore the fatigue life which depends on crack

propagation is less susceptible to differences in the microstructure or surface conditions of the material, which themselves are highly variable. The reduction in scatter is similar to the consistency of results obtained through tensile tests. The preceding equations are also used in conjunction with the AASHTO/AREMA curves discussed later in this study.

2.2.2 Historic Bridge Material, Fatigue, and Wear

During the transition from the 19th to the 20th centuries, bridge engineering became an established profession in its own right and many new books were published on the subject. Additionally, the profession began to transition more from art to science as the understanding of mechanics increased, steel manufacture grew both in quality and quantity, and lessons learned were further communicated through engineering societies of the time such as the Western Society of Engineers. While different areas of bridge design enjoyed different rates of progress, the current discussion deals mainly with steel truss bridges and their constituent materials, similar to the two bridges in the current study.

A seminal work in iron and steel properties was reported by David Kirkaldy in *Experimental Inquiry into the Comparative Tensile Strength and other Properties of Various Kinds of Wrought-Iron and Steel* (Kirkaldy 1862). This work was some of the earliest investigation into providing reference and analysis of metal material properties, seeing as the Bessemer process for steel was only invented in 1855, and the Siemens-Martin Open Hearth process, the kind used to produce steel for the Burlington and Oregon Bridges after that, around 1865. Bridge construction during the 1800s and

onwards has been dominated by Iron and Steel, so Kirkaldy's work is important to the understanding of materials during the period, however the lack of standardization is noted. In fact, George Morison was one of the early advocates for material standards precisely because he saw the value and lack of any such organization (Cooper 1890). It was around the turn of the century that material standards started to form, partly due to Morison's and August Wöhler's advocacy for such.

The engineer J.A.L. Waddell states that in the term between 1850 and 1860, "rational design [of American bridges] really began," (Waddell 1916). One of the first comprehensive books detailing bridge design was *General Specifications for Iron and Steel Railroad Bridges and Viaducts* by Theodore Cooper. F.C. Kunz published a guide for engineers on the design of steel bridges (Kunz 1915). One of the more iconic publications on bridge engineering was published by Waddell himself, *Bridge Engineering* (Waddell 1916). His two volume work contained best practices of bridge engineering from the author's own experience, organized into a specification format. This is a theme of early bridge literature published that it was eminently practical, which suited the state of knowledge and the needs of the day.

The drawback to this early work is that it did not rely much on standardization. The materials used in the construction of the bridges, while being required to meet some minimum specifications, were still not standardized in any form until ASTM was founded in the early 20th century. One of the precursor organizations to AREMA, the American Railway Bridge and Building Association, was only first founded in 1891. Consistency of results in engineering is of utmost importance, and this key feature was

not always present until the 20th century was well underway. The implications for the present study are that one cannot take historical material documentation for granted, but must be validated by testing where possible and practical. Finally, any results that are obtained for the current study can only cautiously be said to apply to the whole of steel bridges during this period, due to the complexity of the phenomena coupled with the variability that is inherent in non-standardized materials.

As bridge infrastructure is becoming increasingly older in America, renewed interest has been taken to understand the current state and future performance of historic railroad bridges that are still in service. A main part of this problem is understanding the material behavior of the bridge, as documentation is not always available or accurate to current standards. A second line of investigation is to ascertain if the structural behavior of current models mimics the actual field behavior of the bridge, as this cannot be assumed to be true. Once the material properties are accurately known and there is reason to believe that the models follow the actual structural behavior well, then remaining life evaluations and safety evaluations can be performed. While many new techniques are being developed to evaluate historic bridge performance and remaining fatigue life, the current study will provide the most accurate characterization of the bridge materials through destructive testing and through taking measurements of properties that are simply not possible to be taken in service with the current state of technology.

Kelton et al. undertook a material investigation of samples taken from a historic wrought iron bridge (Kelton, Arwade et al. 2011). The study performed statistical

analyses on the variability and predictive ability of material parameters of wrought iron from the bridge, similar to the present study. Perhaps somewhat surprisingly, different bridges were tested and significant differences were detected in their material properties. The material behavior of wrought iron cannot be extrapolated to predict the behavior of steel, and as many historic bridges including the ones currently under study are composed of steel, more investigation is necessary to understand how historical steels behaved prior to material standards.

S.P. Sparks wrote a report on the material evaluation of both iron and steel in historic railroad bridges (Sparks 2008). This study relied exclusively on non-destructive material testing of in service bridges which produced proxy measures of solid properties, and gave the analyst the ability to identify potential problems rather than produce accurate estimates of properties. The approach taken, while useful for in-service bridges, does not represent the most accurate method of material characterization for all bridge components, including critical components. Proxy measures are never substitutes for the measurement of the actual quantity. The author is right in asserting that material coupons removed from a bridge at non-critical locations does not represent a precise measurement of the bridge's properties, however the destructive testing is currently the most accurate method and is the one employed in the current study.

Delgrego et. al. studied a steel truss bridge with a very similar configuration to the Burlington Bridge (DelGrego, Culmo et al. 2008). No fatigue properties were directly investigated but the findings of the study have an indirect effect on fatigue. This study made several important conclusions. First is that the measured eyebar stresses

significantly differed from the expected stress distribution obtained through mathematical analysis. Secondly, not all members in a joint are equally engaged in force resistance. Inspections of joints of the in service bridge were carried out and significant wear leading to elongation of the holes was identified. This wear was conjectured to be a contributing cause for the unequal load sharing of eyebars in a joint. However, this wear was only characterized in a qualitative nature and not quantitatively as the bridge was in service. A clear quantitative description of wear is necessary to advance knowledge of the aging performance of the bridge, which the current study provides. Understanding of wear may possibly shed light on the uneven distribution of stresses in joints, if it can be shown that the same phenomenon occurred in the bridges under question.

Uneven stress distribution in steel truss bridges has also been observed in other studies (Bakht and Jaeger 1990). Bakht and Jaeger did not conclude that the uneven stress distribution was due to wearing of the joints, however they did conclude that the difference between members was enough that any analysis of a two eyebar member span should only include one member in the stress calculation. Interestingly, Waddell, in a side comment during discussion on the importance of bridge specialists, mentions uneven stresses due to erroneous design (Waddell 1916). The particular case mentioned was the design of a bridge that did not allow eyebar diagonal lengths to be adjusted, leading to the conclusion that some of the diagonals would be loose and others overstressed according to the design because shop work at the time could not provide the precision necessary. The current study will investigate these phenomena and attempt to provide explanation.

2.2.3 Current Fatigue Design Practice

It is instructive to note the current fatigue design practice of railroad bridges, in contrast to the non-existent fatigue design of turn of the century bridges. The occurrence of fatigue was a byproduct of the new iron and steel world that the Industrial Revolution created. Therefore, fatigue was only just starting to be understood as an engineering phenomenon during these bridges' construction. While the current state of the art does not allow for precise fatigue life predictions, the design procedures developed to date have been highly successful (Schijve 2009). Current fatigue design of bridges is governed by the AASHTO LRFD bridge design specifications as well as the AREMA Manual for Railway Engineering in the specific case that the bridge carries rail traffic, as did the two bridges in the proposed study (AASHTO 2014, AREMA 2014). These specifications incorporate the use of S-N curves as established by extensive laboratory testing (Keating and Fisher 1986). In the AREMA code, the main factors of consideration for fatigue design at a local point on the bridge are as follows: Number of stress cycles N, magnitude of the stress range (the maximum stress – minimum stress), and the fatigue detail category the location or connection falls under. The loading used to determine the stress range is the bridge live load, mean impact load, and centrifugal load. The design stress range S_R is not allowed to exceed the allowable fatigue stress range, S_{Rfat} as outlined in AREMA Tables 15-1-9 and 15-1-10, depending on the Detail category.

$$S_R \leq S_{Rfat} \tag{4}$$

The purpose of this design requirement is to give infinite fatigue life to the bridge. The AREMA manual makes no distinction between allowable fatigue stress ranges for different steel types, but rather treats it as one homogenous material allowable. In the case of our two bridges, there is no evidence to say that this does not hold true.

Eyebars fall under fatigue design category E, a relatively low fatigue strength detail. In the case of the Burlington Bridge, the span between bridge piers is 246 ft, however that span is portioned into nine panels of 27’ - 4” each. Additionally, the diagonal tension members never reach a length greater than 68’ - 6”. Therefore the span length L falls under the less than 100 ft category which gives $N \geq 2{,}000{,}000$. This provides a fatigue threshold of S_{Rfat} = 4.5 ksi, where the stress is calculated either by the effective net area or the effective gross area. Eyebars are susceptible to crack formation in the area fanning out from the transverse sides of the head (Figure 2-4).

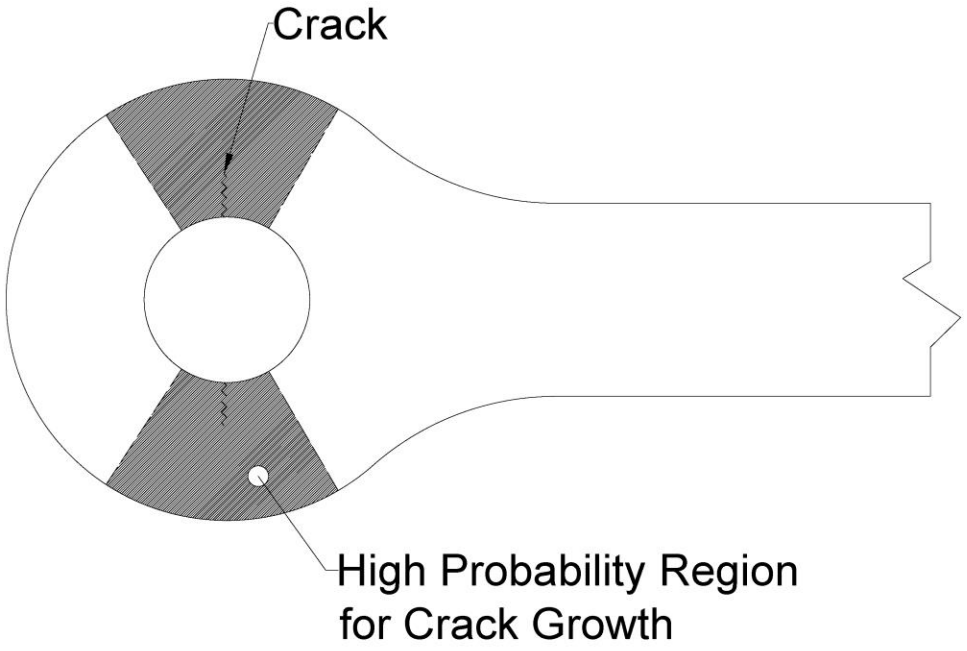

Figure 2-4 – High Probability Region for Crack Growth

AASHTO contains similar provisions to AREMA. AASHTO curves serve as the basis for AREMA fatigue design. The fatigue performance of these period bridges will be investigated and compared to the current AREMA fatigue design provisions.

To the author's knowledge, no comprehensive study of eyebar fatigue or eyebar hole wear has been performed to date. The current study represents a new addition to fatigue literature. It is possible that the lack of studies surrounding eyebar fatigue is due to the fact that they are seldom the most critical fatigue feature of the bridge, nor the site where fatigue cracks nucleate and propagate most often. The fact remains that eyebars fall under Fatigue Category E in both the AASHTO and AREMA manuals, which is one

of the worst fatigue design category. However, as noted earlier by multiple authors, the behavior of 19th century bridges often yields surprising results that deviate from expectation (Bakht and Jaeger 1990, Kelton, Arwade et al. 2011). The current study will fill in some of the gaps in the literature surrounding eyebar fatigue and material performance of early railroad truss bridges. With the increase in rail loading beyond what these bridges were designed to carry, and the effects of corrosion, wear, and possibly, less than ideal design and construction practices of these early bridges, thorough knowledge of their behavior is paramount to continued rail infrastructure safety. Engineers and policy makers will be able to use the results of this study to make more economical and safer decisions in the future.

CHAPTER III

EXPERIMENTAL METHODS

3.1 Extraction, Cleaning, and Measurement

Eleven joints were obtained for testing from the Burlington and Oregon Bridges together. Though the eyebar bridge joints are designed as pin connections, the state that they were in when the eyebars were first extracted from them was in some cases closer to a fixed joint due to the corrosion of the material. It is unclear whether this fusing corrosion occurred before or after the bridge demolition, but it is highly probable that it occurred after joint removal due to the length of time between demolition and testing and the combined effects that removal of the joint and transportation would have on them. Sledgehammers up to 20lbs in weight, levers, wedges, come-alongs, WD-40, and heating techniques were used to loosen the eyebars and remove them from the joints. Care was taken to impart as little damage as possible when extracting the eyebars, however some eyebar cut ends were physically deformed from the sledgehammers and subsequently removed before testing after the eyebar was free of the joint. The maximum temperature applied to the eyebars was 400℉. Plastic deformation was avoided, and eyebars that could not be procured were simply left out of the test dataset. A number of eyebars were bent during the demolition or were cut too short to use for anything other than wear measurement. Figure 3-1 shows a representative scene during the joint extraction process.

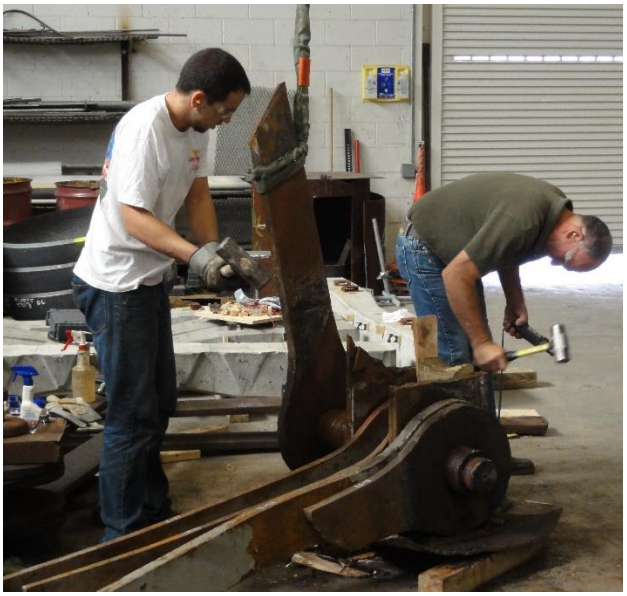

Figure 3-1 – Eyebar Joint Dismantling

After the eyebars were removed, they were subsequently cleaned and checked for defects, flaws, and cracks. The faces of the eyebar head were scrubbed clean of rust and paint as much as could be done without affecting the metal underneath. Dye penetrant tests were performed on the faces to locate any surface cracks in the region of high crack probability. The eyebar head faces were very pock marked but no surface cracks were located with the dye penetrant test. An Olympus phased array module was employed to scan the eyebar heads for any faults or cracks as well and some were found. Eyebars were distinguished by joint and bridge using the following rationale.

1. Joint naming convention – we have the plans for Burlington Bridge, and on it are marked eyebars with U8, M8, etc. All of those joints with these designations look the same.

2. The joints that don't have similar names as U8, M8, etc. have a coat of silver paint applied, indicating they are from the Oregon bridge.
3. Historic photographs of the Burlington Bridge do not reveal silver or light colored paints on the steel members. The color of the bridge members in the available photographs is consistent with the color of the eyebars obtained in the laboratory.
4. The Burlington bridge specification calls for a coat of Cleveland iron clad paint, purple brand, to be applied. Assuming that "purple brand" indicates the color and nothing else, we can say that those eyebars without the silver paint are from Burlington. Even if that is not the case, a review of historic Iron Clad paint advertisements does not reveal silver or white as a color choice, however purple-brown is, which could possibly be the "purple brand" referred to by Morison in the bridge specification.

Wear measurements were taken on both the eyebar head hole and on the pins themselves. The purpose was to quantify the average wear at the two locations. The main cause of wear is determined to be fretting wear. In summary, the eyebar heads showed larger wear values relative to their original diameters whereas the pins showed smaller wear values, with large variability in both measurements.

Hole wear measurements for the eyebars were taken by measuring the gap between a 6 in diameter disc and the wall of the eyebar hole as shown in Figure 3-2.

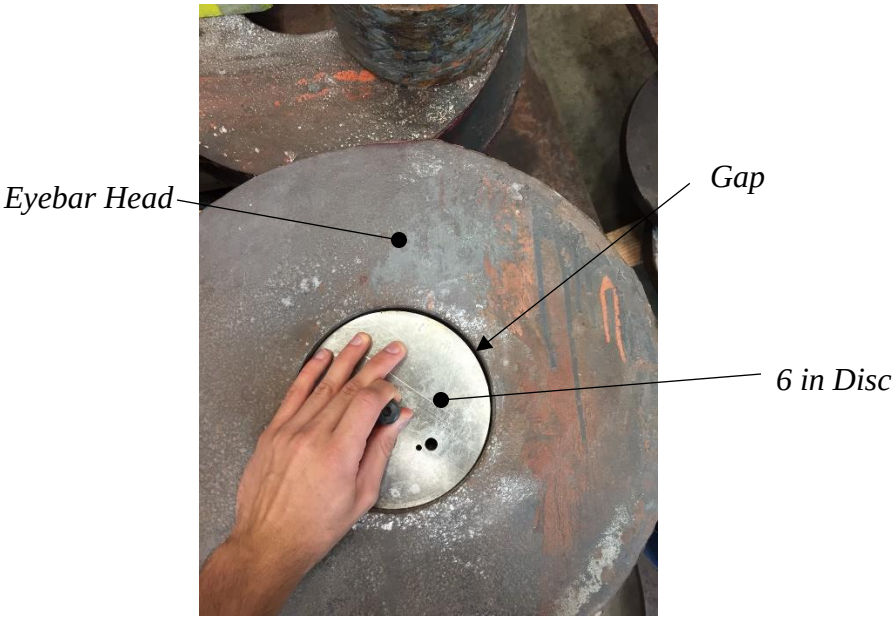

Figure 3-2 – Wear Measurement Procedure

Wear measurements for the pins were taken first by measuring the circumference of the pin at locations along its length and calculating the diameter to be circumference / π. The wear value was calculated by subtracting the diameter from a 6 in nominal diameter.

3.2 Fatigue Testing Procedure

After cleaning and measurements were taken on the eyebars, eyebars in the best condition were selected for fatigue testing. A 1500 kip capacity MTS test frame was employed in the Structural and Material Testing Laboratory of the Zachry Department of Civil Engineering, Texas A&M University in College Station, TX to fatigue test the eyebars. The 1500 kip frame was designed with interlocks to shut down automatically if the eyebar fractured or there was a mechanical/electrical problem that occurred. Data acquisition occurred continuously and 1200 cycles of data were saved to a file every 5

minutes during running. The cycles were recorded continuously. A specifically designed clevis and pin were used to attach the eyebar to the machine, the other end gripped in friction as shown in Figure 3-3.

Figure 3-3 – Fatigue Test Setup in 1500 kip frame

The fatigue cycles were then initiated and the eyebar was allowed to run until fracture or until a sufficient number of cycles to establish runout were accumulated. In total, 13 eyebars were fatigue tested. Tests were performed in both the finite and infinite life regions of fatigue. Several times, the machine was tripped for electrical and mechanical reasons and the test shut down temporarily. There was no issue with load

sequencing at this point, because the machine was programmed to shut down automatically.

3.3 Tensile Testing Procedure

In order to determine the tensile yield strength and ultimate strength of the two bridge steel materials, tensile testing was performed on specimens taken from eyebars at the locations shown in figures A-1 and A-2 in Appendix A. After blocks were removed from the described locations, specimens were machined from the blocks in accordance with ASTM E8 standards for tensile testing specimens. In total, 24 specimens were tested at a strain rate of 0.05 in/in/min on an MTS tensile testing machine in the Structural and Material Testing Laboratory. The same strain rate was used in the elastic region as was used in the strain hardening and ultimate strength regions. All specimens were tested to ultimate failure. Figure 3-4 shows a typical tensile testing setup using the MTS machine.

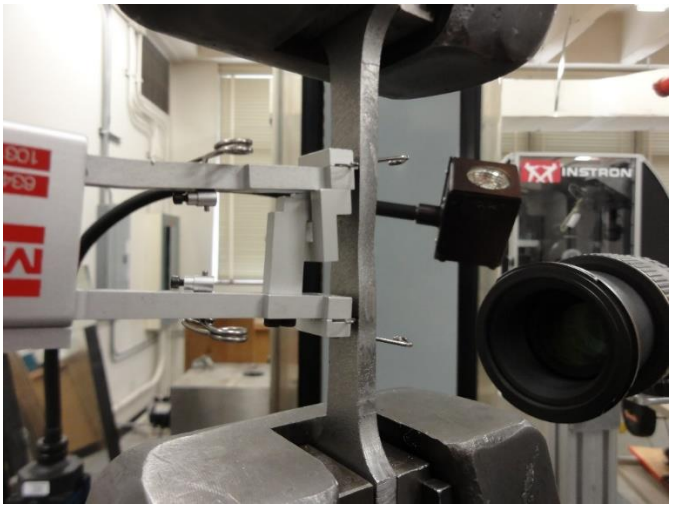

Figure 3-4 – Tensile Testing Setup

3.4 Data Analysis

After testing was complete, several datasets became available for analysis. These included the sample of wear measurements, the fatigue cycles to failure, and the general eyebar measurements taken. The main tools used to analyze these datasets are Matlab and Microsoft Excel. Analysis of Variance Testing has been carried out in Excel on several different samples from the experiment. Distribution Fitting and Histograms are calculated in Matlab. Both programs are used to produce plots of the data. See Appendix C for a listing of the Matlab code used to generate the tests and plots.

CHAPTER IV

EXPERIMENTAL RESULTS

4.1 Wear Measurements Results

The histogram shown in Figure 4-1 is skewed right and shows the wear data clustering towards small wear values. Inspection of the histogram data shows that only 38.1% of the wear values fall above the mean of 0.121 in, and correspondingly 61.9% fall below the mean. This shows the heavy influence of the tail data, not only for the mean, but in the later choice of distribution testing to identify the underlying statistical distribution (See Section 4.3). The data suggests very little differential movement between the eyebar and pin, i.e. small deflections because of the 100+ year service life as expected. The assumption that the pin and eyebar are constructed of the same material is verified through inspection of the specification from George Morison (Morison 1893). Dismantling of the bridge joints has shown extensive rusting between the eyebar heads and pins which has fused the two pieces together and has sometimes required large impact forces and the application of up to 400 °F of heat to loosen, being careful to avoid plastic deformation of the member. This corrosion joining some of the eyebars to the pins most likely occurred after the joint was removed from service. Table 4-1 provides summary statistics of the eyebar wear and pin wear.

The credible mechanisms for wear of the eyebars are corrosion and differential movement from deflections causing friction to wear away the material, also known as fretting wear. Due to the choice of pin joints, fretting wear is a viable wear mechanism.

Most of the joints examined had extensive corrosion locking the pieces together which had to be overcome. A knowledge of the past deflection history, material properties of the steel, and any coating protection will help to understand the most dominant wear mechanism that operated during the service life of the bridge, approximately 117 years, plus the multiple years of storage time before the joints were secured for the project.

Table 4-1 – Wear Measurement Results

	Mean Wear (in)	Std. Dev.	Coefficient of Variation	Max Value
Eyebar	0.121	0.106	0.883	0.340
Pin	0.036	0.045	1.247	0.064

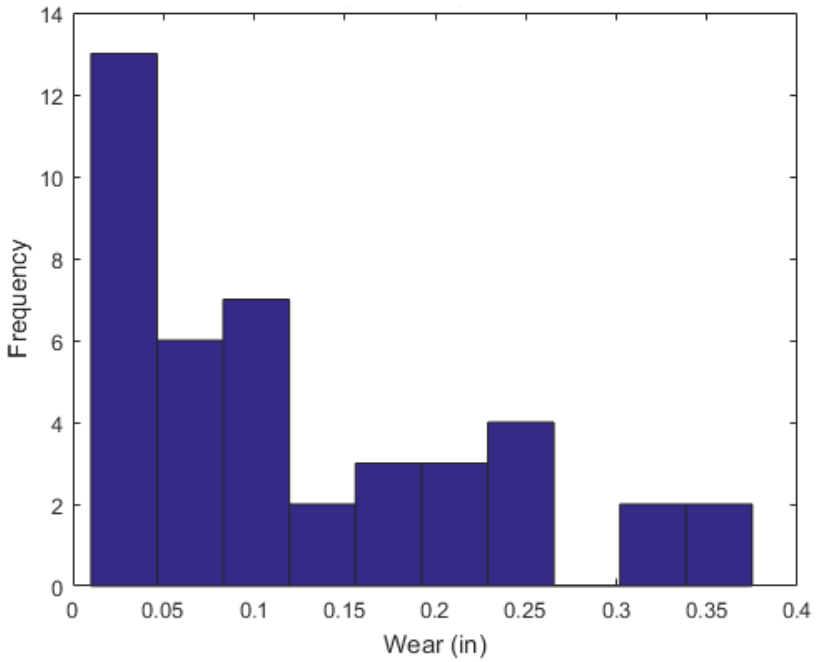

Figure 4-1 – Histogram of Eyebar Wear

4.2 Statistical Considerations

It is clear that, overall, the eyebars have worn more than the pins themselves, though their wear is more even in nature. An Analysis of Variance test (ANOVA) test of the eyebar hole diameter measurements, shown in Appendix B indicates that there is no statistically significant difference in the diameters of the eyebars in the longitudinal and transverse directions (p=0.84 Side A, 0.92 Side B). ANOVA is robust to deviations from normality and is a good choice for testing the two sample means. The analysis indicates two things.

1. The measurement of wear based on the gap between a 6-inch diameter disc and the eyebar hole will not on average differ based on the location around the circumference of the hole at which the gap measurement is taken. This fact is established through ANOVA test of the longitudinal and transverse diameter measurements, which shows no discernable difference in the two samples. This is important because it proves that even wear has occurred on the eyebar hole. If the wear were uneven, we would expect a difference in the two measurements.
2. No plastic deformation of the eyebars in the longitudinal direction will affect the hole wear measurements. For example, if the eyebars had been subjected to a large enough tension stress along their longitudinal axes during their service life to produce plastic deformation, it would have elongated the eyebar hole (analogous to Poisson's ratio) to produce an approximate oval shaped hole, which would give different diameter measurements along the transverse and

longitudinal axes. Though this phenomenon is possible in a few number of eyebars in our sample, the fact that there is no statistically significant difference between the two groups shows that in the average of individual eyebars, this is not the case. Interpretation of the magnitude of the wear data also supports this conclusion. Finally, no eyebar measured showed greater than 3.2% deviation between the longitudinal and transverse directions of measurement.

Finally, it must be noted that the sample size of pins is much smaller than the eyebars (42 vs 4), and there is much greater variability in the measurements. Reasonable conclusions cannot be drawn from the pins at this time since the sample size is too small.

4.3 Distribution Fitting

In order to model the eyebar hole wear data properly, a random variable will serve as a mathematical characterization of the inherently random phenomenon of wear. From the observed data, one can determine if these data points can be described by already established, well known probability distributions. In order to answer this question, several probability distributions are tested against the wear data using an Anderson-Darling test. The Anderson Darling (AD) test uses the EDF to measure the deviation between the data and the hypothesized distribution, with the addition of a weighting function as

$$n\int_{-\infty}^{\infty}\left(F_n(x)-F(x)\right)^2 w(x)dF(x) \tag{5}$$

where $F_n(x)$ is the EDF, $F(x)$ is the hypothesized distribution function.

Additionally, $w(x)$ is the weighting function defined as

$$w(x) = \frac{1}{F(x)(1 - F(x))} \tag{6}$$

The AD test is more sensitive to deviations in the tails of the distribution than other goodness of fit tests due to the presence of the weighting function. Therefore, it has been selected as best choice for evaluating the distributions since by inspection they are skewed. These distributions are selected due to their approximately equivalent shape to the histogram of the sample data, which is the first fitting step. The goodness of fit test is evaluated at $\alpha = 0.05$, consistent with Fisher's criteria. A *p* value less than α will cause us to reject the null hypothesis (H_0), the wear data follows the chosen model, and accept the alternate hypothesis (H_a), the wear data do not fit the chosen model. The interpretation of the *p* value is that given the null hypothesis is true, what is the chance of seeing a sample like the one observed? Table 4-2 and Figure 4-2 show the results of the distribution fitting procedure.

Table 4-2 – Anderson Darling Hypothesis Test Output

Model	***p* Value**	**AD Statistic**
Weibull	0.1944	0.5137
Lognormal	0.0777	0.6623
Exponential (Best Fit)	0.5828	0.4387

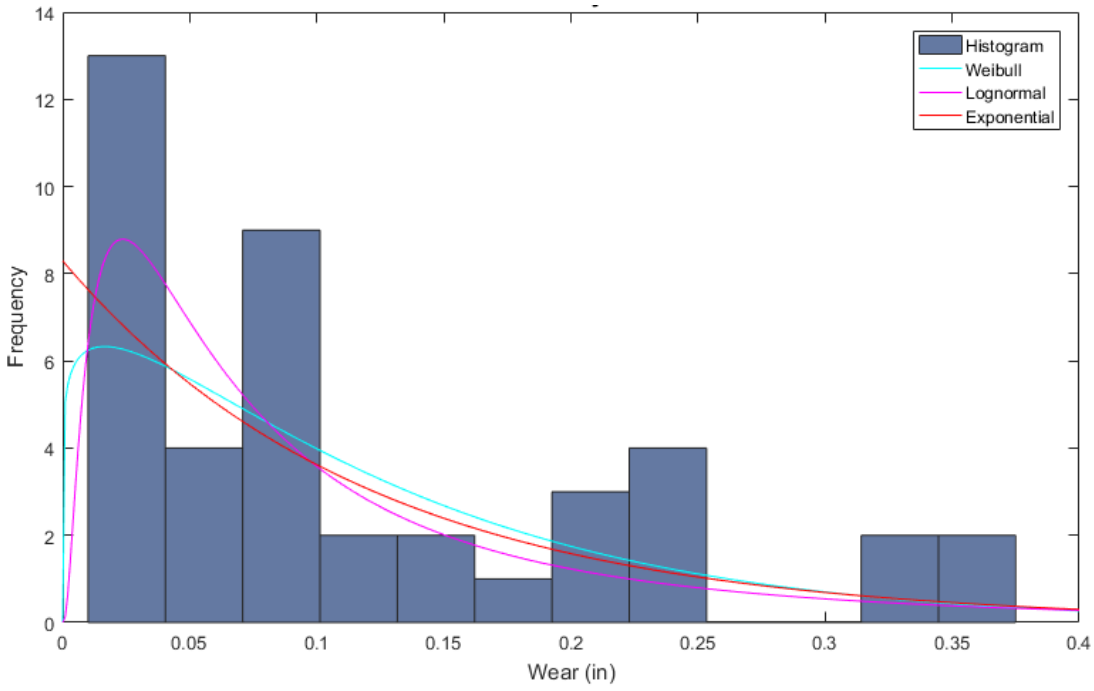

Figure 4-2 – Distribution Fit of Eyebar Wear Data

The Anderson – Darling test results show that the exponential distribution gives the best fit of our chosen models. The model not only relatively is better than the other compared models, but it gives a good objective fit for the data. The exponential distribution has the smallest AD statistic, the highest *p* value, and the best fit on a probability plot of any of the evaluated distribution. We also see that the Weibull is superior to the Lognormal. This can also be seen in Figure 4-2. Figures 4-3 and 4-4 show the probability plots for the lognormal and exponential distribution, respectively.

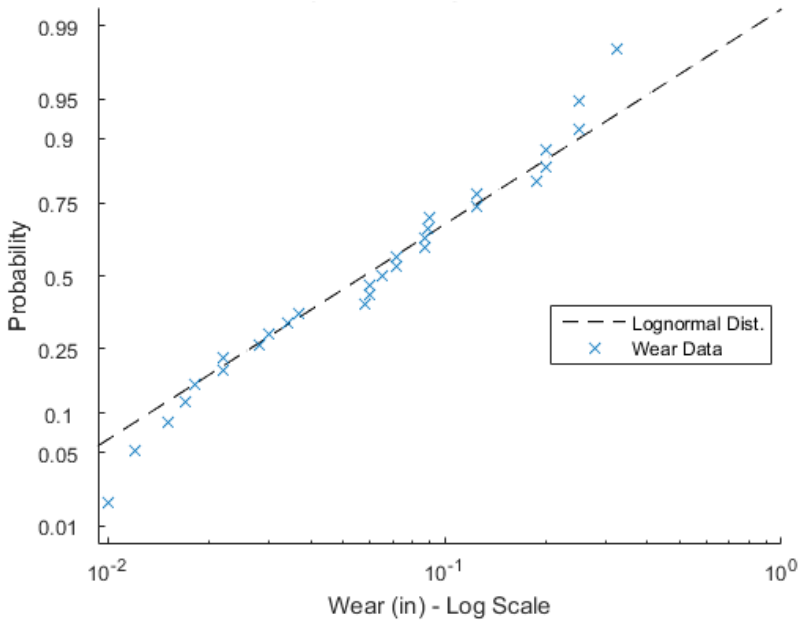

Figure 4-3 – Probability Plot for Lognormal Distribution

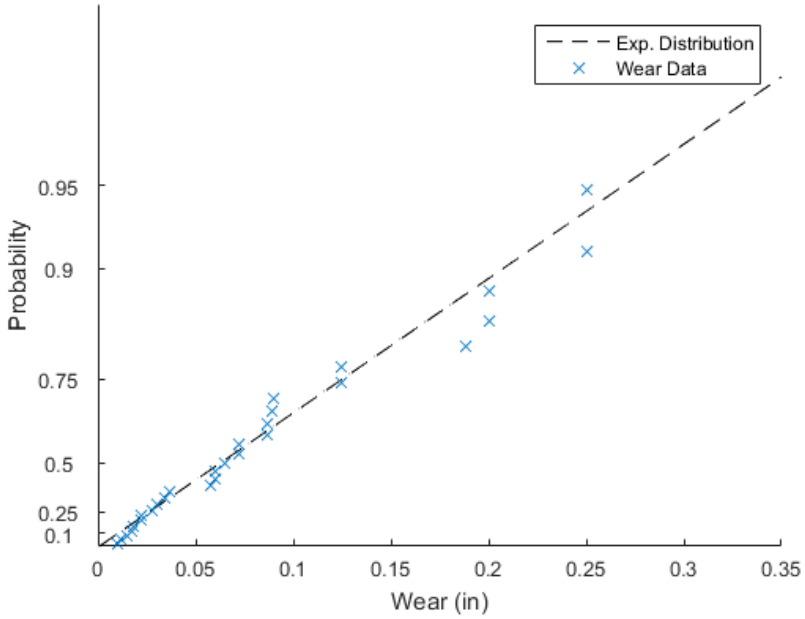

Figure 4-4 – Probability Plot for Exponential Distribution

In light of the preceding discussion, the exponential distribution was chosen as the best distribution to model the wear distribution of these period bridges. The exponential probability distribution function has the following form

for all x in (0, ∞)
$$f(x;\lambda) = \begin{cases} \lambda e^{-\lambda x} & x \geq 0 \\ 0 & x < 0 \end{cases} \quad (7)$$

If mean μ = 0.121 in, the wear fitted rate parameter λ is:

$$\lambda = \frac{1}{\mu} \sim 8.295 \quad (8)$$

The fitted distribution then takes the following form:

$$f(x;\lambda) = 8.295 * e^{-8.295*x} \quad (9)$$

The 95% confidence interval for the mean, μ of the population of wear data is:

$$0.0910 < \mu < 0.1673 \quad (10)$$

Note that the 95 percent confidence interval does not mean that there is a 95 percent chance that the mean is between the two end values, rather that the algorithm used to create the interval from the sample data will include the mean 95% of the time. There is no guarantee that the current interval does contain the mean. If we were to repeat our sampling and generate a confidence interval 100 times, 95 of those confidence intervals would contain the population mean. In order to obtain a true probability interval, a Bayesian approach must be taken, however a Bayesian framework is left out of the current discussion. It must also be noted that since this is a continuous probability distribution, point estimates of probability are not possible due to the infinitesimal nature of the distribution and the zero probability of obtaining a specific value.

The fitted distribution will allow us to make future probabilistic predictions about the eyebar wear. For example, using the quantiles of the cumulative distribution function for the exponential function, one can infer that 99 percent of the wear values of all eyebars taken from turn of the century railroad bridges are between 0.0 and 0.555 inches.

4.4 Material Testing

Tensile tests, and material composition tests were run on selected specimens taken from each bridge. Specimens taken from the eyebars and pins of both bridges were sent to a material testing laboratory for analysis. Figure 4-5 shows a typical tensile specimen after testing. The original construction specification cites that the bridge in the most part, excepting…., was constructed with medium steel (Morison 1893). Both the acid and basic open hearth processes were utilized to produce the steel of the Burlington Bridge. While ASTM standards were not written until 1898, five years after the Burlington Bridge construction, the behavior of the Burlington steel still shows some patterns.

Figure 4-5 – Tensile Test Specimen after testing

Initially, a sharp difference was noted in the tensile test results for specimens taken from the side of the eyebar head vs the neck area. The neck area showed much higher yield strength and ultimate strength than did the side areas. More specimens were prepared to verify this pattern, however no correlation was found with subsequent testing.

The naming convention for the tensile specimens follows the pattern Joint #-Eyebar#-Specimen #. Where the specimen is part of multiples batches taken from the same eyebar at different locations, the pattern is Joint #-Eyebar#-Location#-Specimen #. Figures 4-6 and 4-7 show the tensile yield strengths and ultimate strengths respectively of the Burlington and Oregon Bridges. Table 4-3 shows the results of all material tests.

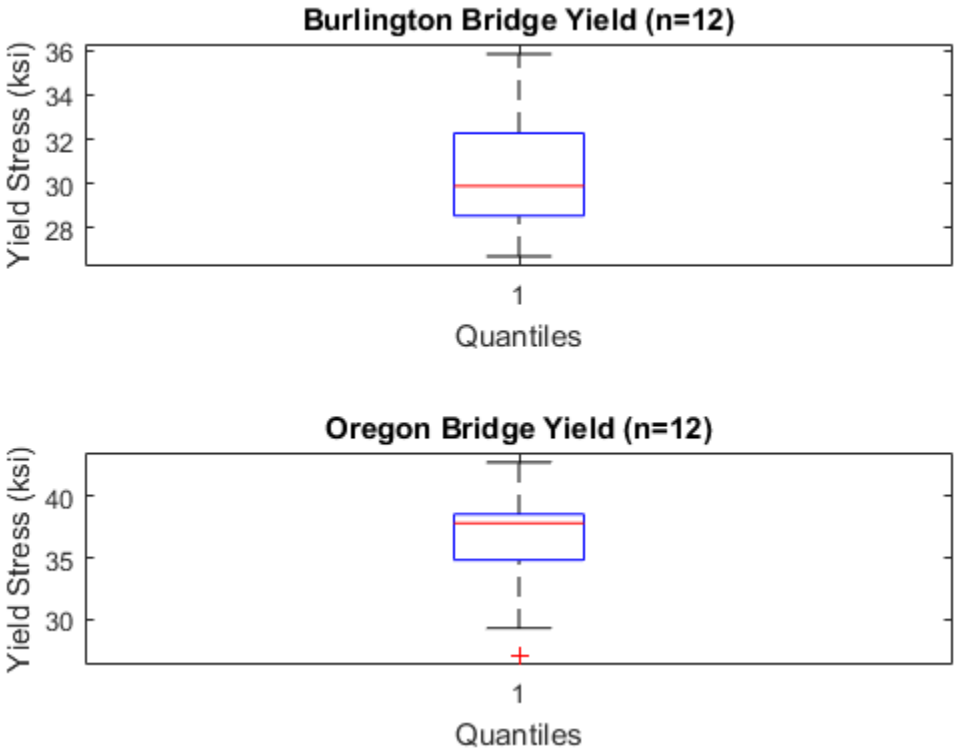

Figure 4-6 – Boxplot of Tensile Yield Stresses

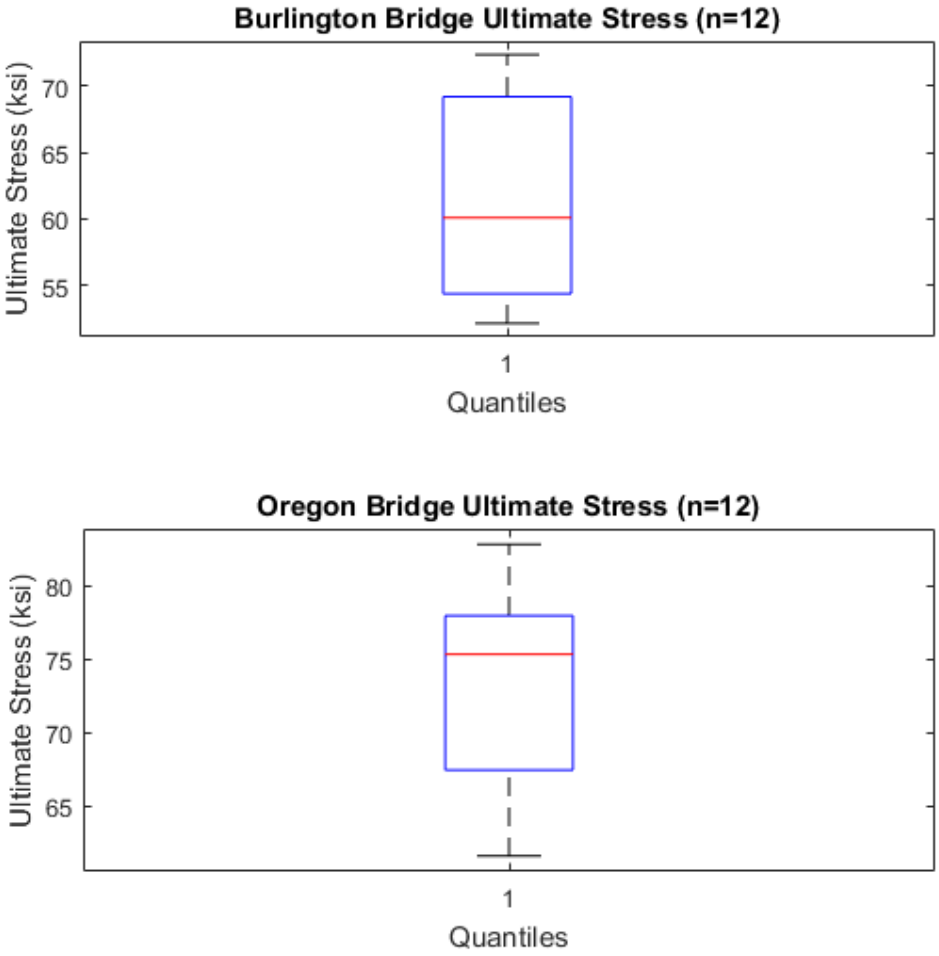

Figure 4-7 – Boxplot of Ultimate Stresses

Table 4-3 – Material Test Results

Specimen	0.2% Yield Stress, ksi	Ultimate Stress, ksi	E, ksi	%Elongation
FT-00-1	31.9	67.3	28525	0.23
FT-00-2	29.3	64.0	17634	0.30
FT-00-3	30.9	65.1	11189	0.36
11-7-1	27.1	61.6	27936	0.37
11-7-2	37.4	80.0	25314	0.27
11-7-3	29.3	62.8	30879	0.29
FT-01-1	35.9	71.9	19541	0.26
FT-01-2	33.7	71.1	27200	0.39
FT-01-3	32.7	72.4	26765	0.37
FT-03-1	28.6	52.1	30726	0.21
FT-03-2	29.0	54.1	20820	0.22
FT-03-3	30.5	52.7	31403	0.22
FT-04-2	26.7	56.0	22211	0.33
FT-04-3	26.7	54.7	23556	0.32
FT-04-4	28.5	56.2	28588	0.41
11-9-1-1	34.8	67.9	25873	0.23
11-9-1-2	39.9	79.1	22823	0.18
11-9-1-3	42.7	82.8	29043	0.10
11-9-2-1	38.5	76.7	24307	0.17
11-9-2-2	34.8	67.3	26309	0.26
11-9-2-3	37.7	74.6	27030	0.13
11-9-3-1	38.3	67.6	26137	0.25
11-9-3-2	38.6	76.1	19574	0.10
11-9-3-3	37.9	76.8	28916	0.20

Burlington Bridge appears to be constructed of steel similar to ASTM A7 type steel, while the Oregon Bridge shows behavior close to A36 steel. Both bridges have an ultimate tensile strength that is approximately twice that of the tensile yield strength. The material strengths of turn of the 19th century bridges are shown to be highly variable.

According to the Burlington Bridge Specification prepared by the chief engineer, medium steel used in the construction of the bridge was to have a minimum tensile yield strength and ultimate tensile strengths of 38 ksi and 65 ksi respectively. Surprisingly, the data show a different picture. The found strengths were 30.4 ksi and 61.5 ksi. The requirement of at least 20% elongation was met, especially given that many of the tensile specimens broke outside of the gauge length, which tends to reduce the figures for percent elongation.

It is possible that higher strain rates of early testing machines are responsible for a small part of the difference between the Burlington Bridge specification and the test results. Loveday makes the point that depending on the test machine used in the 19th century tests, strain rate may not have been controlled well at critical points, such as the first drop in load at the lower yield point (Loveday, Gray et al. 2004). This could produce strain rates that were in excess of what is considered standard today and consequently produced somewhat inflated values of the static yield stress. It is known that according to the Burlington Specification written by Morison that eyebars and eyebar materials were required to be tested at certain intervals prior to shipment, but the quality of the test machines or their configuration cannot be verified.

It has also been noted in previous research that the level of precision of early testing machines before the development of precision hydraulic, screw driven, and servo controlled machines was not at the quality level it is today. In light of these facts, it can be deduced that the observed difference in the yield strength of Burlington Bridge specimens and the required yield strength as written in the bridge specification are in

part due to different strain rates applied and differences in test accuracy. It is ironic that one of the bridges designed by an early champion of material testing should turn out to have a strength much lower than expected, but the current data show this to be the case.

4.5 Stress-Strain Curves

Figures 4-8 through 4-11 show the stress-strain curves of eyebars that were fatigue tested. Note that all stress-strain curves generated in this research show engineering stress, not true stress.

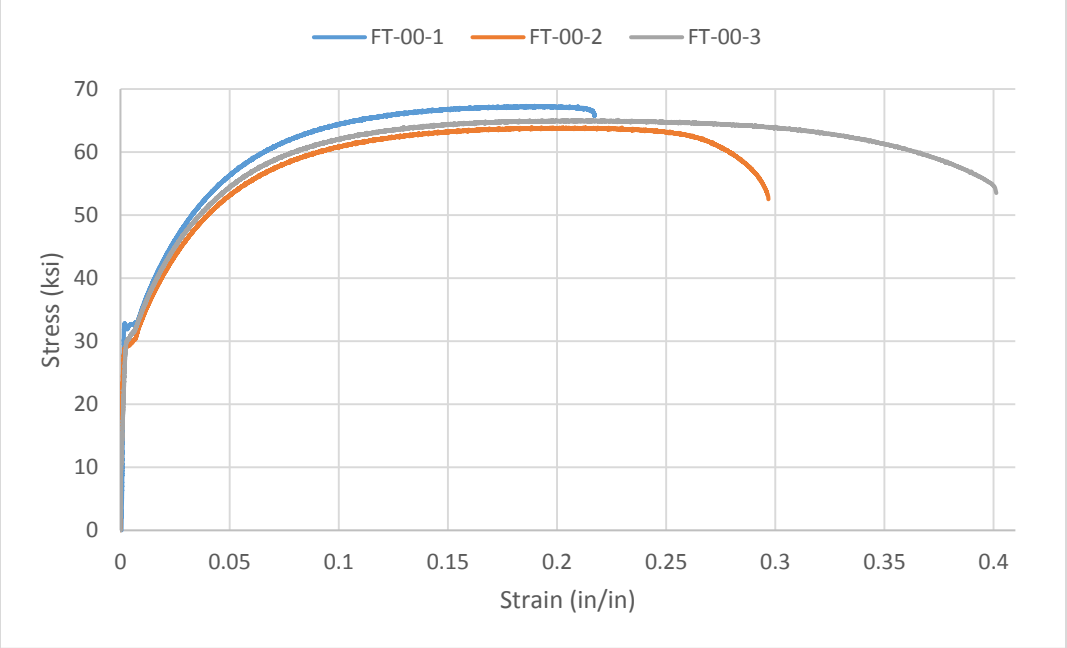

Figure 4-8 – FT-00 Stress-Strain Curves

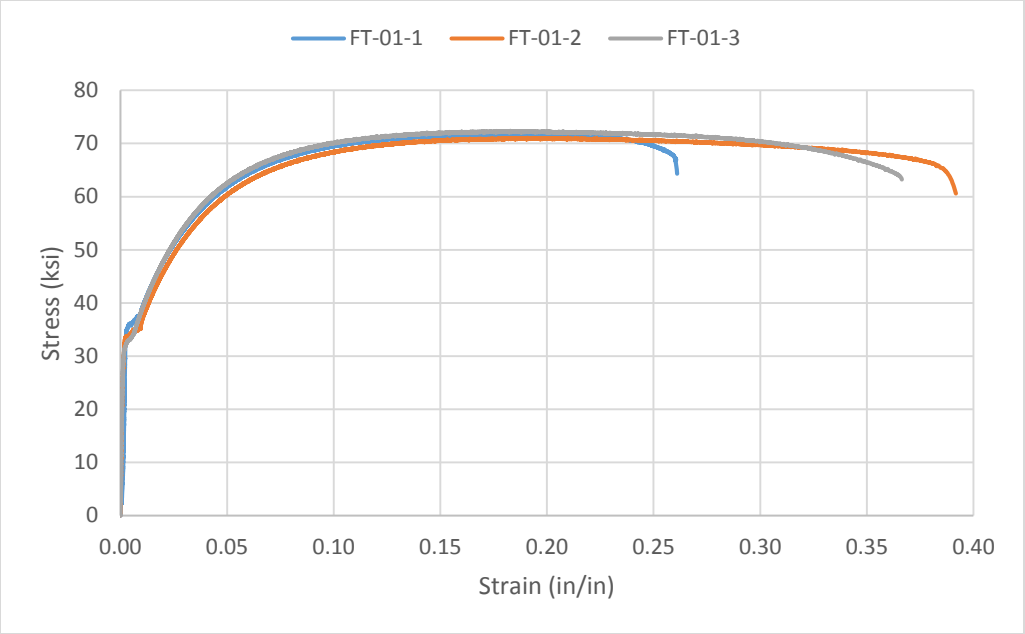

Figure 4-9 – FT-01 Stress-Strain Curves

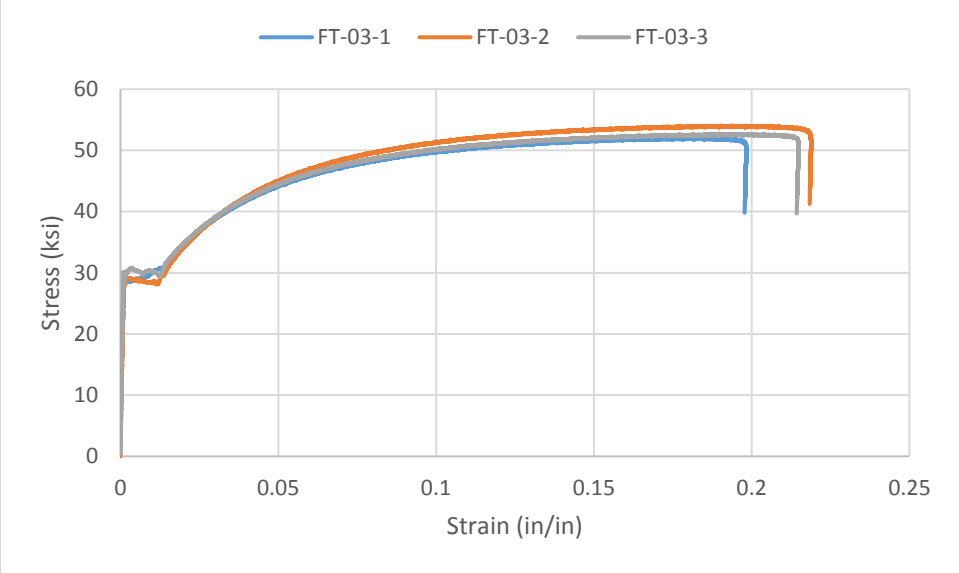

Figure 4-10 – FT-03 Stress-Strain Curves

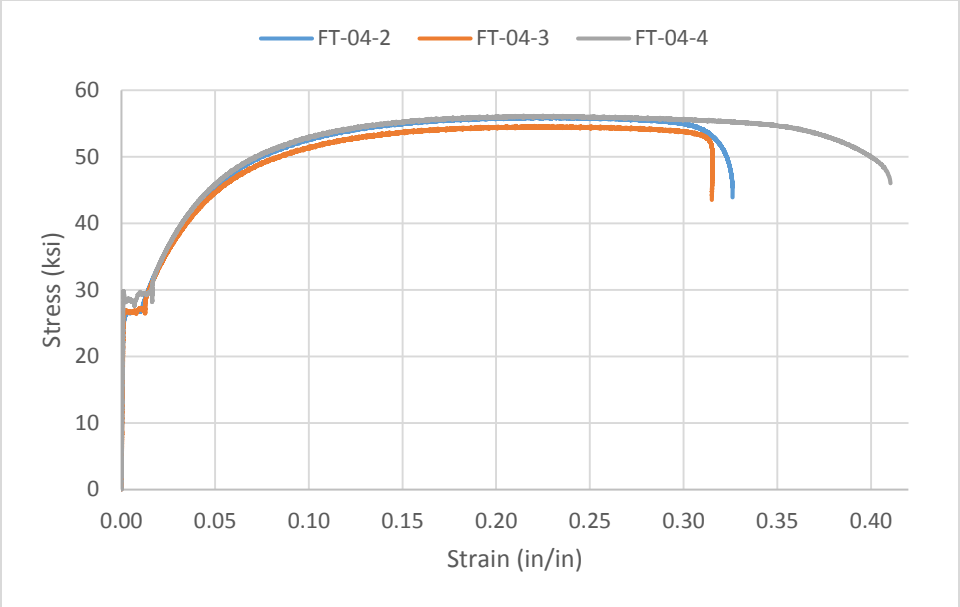

Figure 4-11 – FT-04 Stress-Strain Curves

4.6 Fatigue Behavior

Figure 4-12 and 4-13 are plots of the fatigue test data from this study with AASHTO Fatigue Design Curves C, D, and E. Table 4-4 shows the fatigue test data for all specimens. Overall, the eyebars showed interesting fatigue behavior that deviated from the AASHTO fatigue design criteria. Refer also to Section 5.3 for in depth discussion of the fatigue test results.

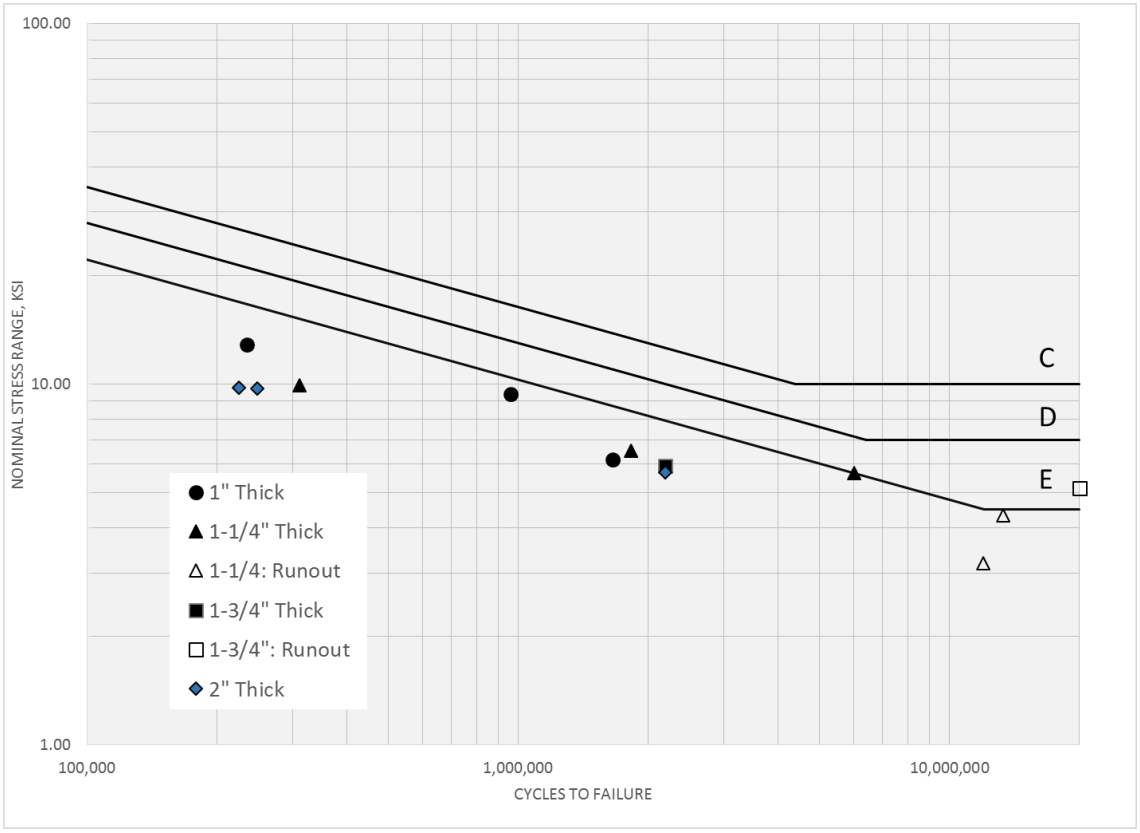

Figure 4-12 – Eyebar S-N Curve by Thickness

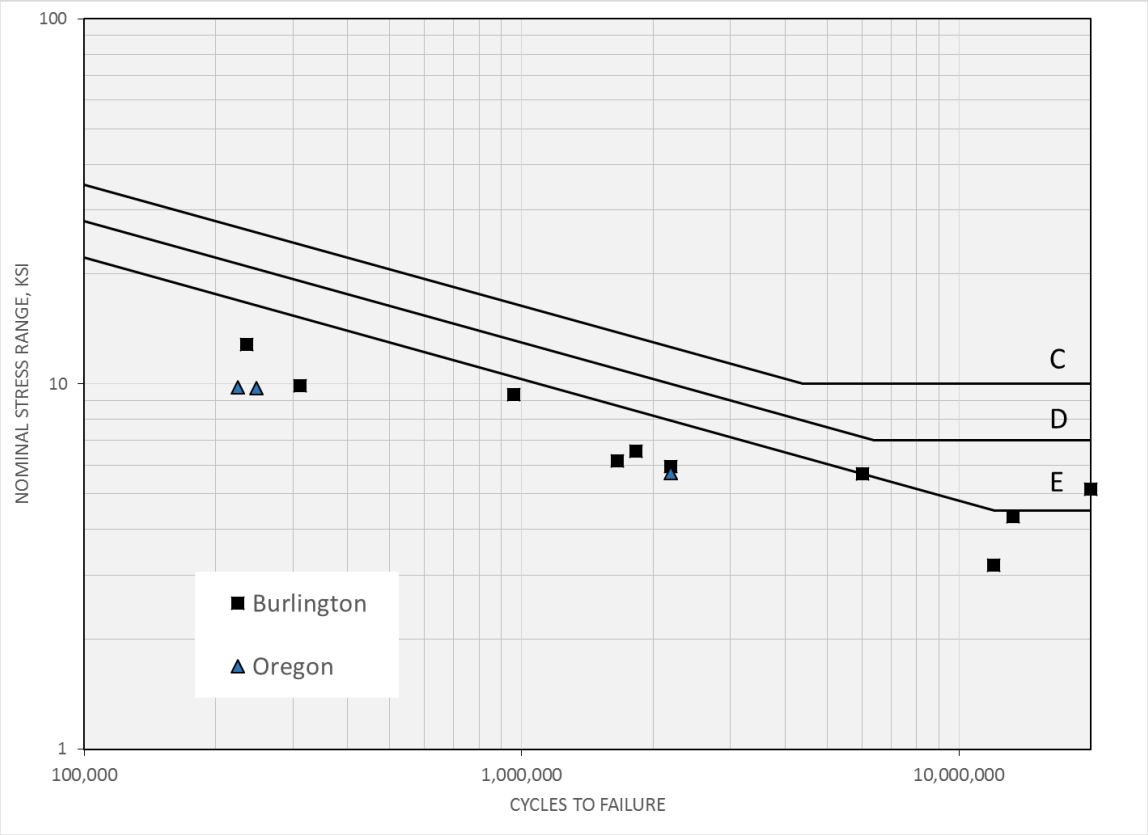

Figure 4-13 - Eyebar S-N Curve by Bridge

Table 4-4 - Eyebar Fatigue Test Results

Eyebar	Stress Range, ksi	Cycles to Failure
FT-00	12.85	235,175
FT-01	9.38	960,762
FT-02	9.79	224,861
FT-03	6.17	1,656,031
FT-04	6.55	1,826,938
FT-08	3.20	12,000,000
FT-06	9.92	311,153
FT-07	9.73	248,061
FT-08	4.33	13,302,022
FT-09	5.67	6,012,200
FT-10	5.86	2,190,320
FT-11	5.95	2,190,000
FT-12	5.14	20,000,000

As expected, scatter was observed in the fatigue results. It is well known that surface finish of a material has a strong effect on the fatigue life of a specimen (Bayoumi and Abdellatif 1995), due to fatigue being primarily a surface phenomenon (Schijve 2014). The scatter expected was increased due to pock marked and corroded surface conditions along the circumference of the eyebar pin holes. The eyebar steels produced a fatigue threshold of at least 5.1 ksi but no greater than 5.6 ksi. The two steels did not show significant deviation in fatigue behavior from each other, despite having two different yield strengths. This is consistent with AASHTO/AREMA fatigue design which does not account for steel yield strength when calculating the fatigue threshold. The tested eyebars would meet modern design requirements if designed for infinite life,

since 5.1 ksi is greater than 4.5 ksi. The fatigue test results consistently fall below the Category E design curve, however they show a similar slope as the design curves.

Figure 4-15 shows a simple linear regression computed using the S-N curve data from the finite life region of the curve, meaning that any runout data is not included in building the model.

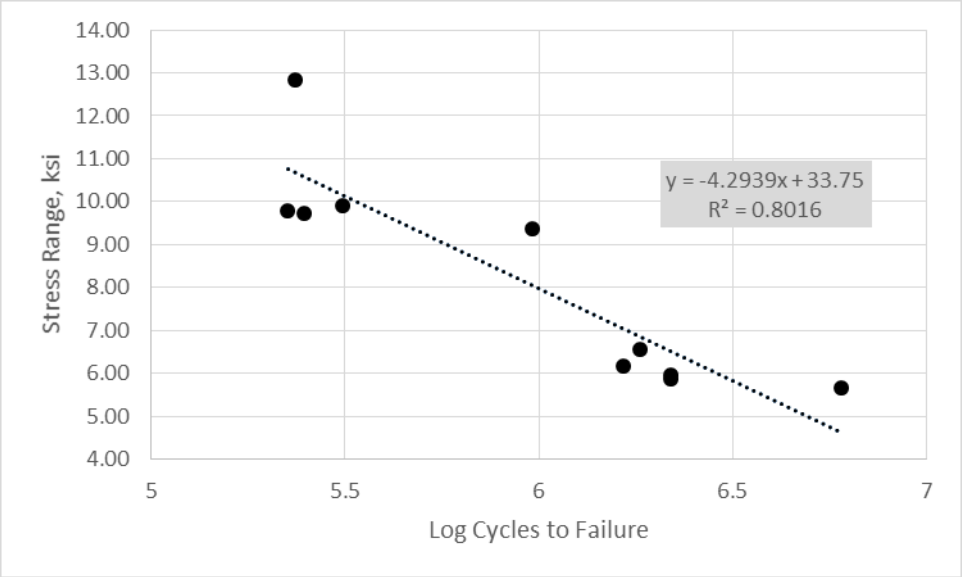

Figure 4-14 - Eyebar Fatigue Linear Regression
Finite Life Region

The model shown in Figure 4-15 can be used to predict future fatigue test results in the finite life region of the curve with reasonable accuracy. The current best estimate of the fatigue threshold for these eyebars is 5.1 ksi, corresponding to the highest stress range in testing that produced a runout.

CHAPTER V

SUMMARY AND CONCLUSIONS

5.1 Inferences from Wear Data

5.1.1 Small Displacements

If the main mechanism of wear is fretting wear, which occurs on a time scale, then we can conclude from the wear data that the joints saw very little differential movement between them and the pin in a qualitative sense. Small displacements, though being expected (and in fact required for the main of structural analysis techniques) can be inferred from the wear values over the 117 year life of the Burlington Bridge and possibly 100 year life of the Oregon Bridge. In turn, the relatively small displacements suggest low stress levels in the eyebars by Hooke's law for the majority of service life, a finding that is supported elsewhere in the body of research on this topic (Fisher, Yen et al. 1987, Åkesson 1994). The findings from the current study support the claim of substantial fatigue life left in historic railroad bridges in America. A more accurate estimation of these stresses can be realized from use of historical traffic data in conjunction with a finite element simulation of the bridges, as recent history has shown a trend towards heavier freight traffic that causes more fatigue damage than earlier freight traffic (Imam, Righiniotis et al. 2005). An accurate simulation of the stress levels in the eyebars would allow for estimation of a normal force at the point of contact between pin and eyebar which would allow some correlation between stresses and wear, which could then be weighed against the fatigue life.

Eyebars in some given joints did not see the same stresses as would be expected due to their configuration. The fact that the wear patterns on the pins inspected were not uniform suggests that some bars were engaged more than others, though it is highly unlikely that this was intended by the designer. This finding supports previous research (Bakht and Jaeger, 1990). Data show that even within a given joint, under the assumption that stress and wear are related through the action of fretting wear, then the eyebars did see uneven stress distributions. Even with this being the case, we can see that the evidence supports low stresses during the bridge service life because of low wear values and the lack of correlation between wear and fatigue failure cycles. We could not necessarily conclude low stresses from high wear values because a small stress applied over time could produce a high wear just as easily as a high stress over low time could. A finite element simulation would provide more evidence to support these claims. The reason for the uniform wear values in the eyebars vs the pins is not known at this time.

5.1.2 Effect of Wear on Fatigue

The current study has shown that uneven wear around the pin hole has not occurred in the majority of eyebars, due to the ANOVA test of longitudinal and transverse diameters showing no significant difference between the two. Even though wear theoretically occurs in a different location than the high probability region of crack growth as shown in Figure 2-4, it is expected that wear and remaining fatigue life will correlate to some degree. This does not necessarily mean that a high wear value is evidence of a high stress value, because a high wear value could be obtained from a low

stress applied over a long timeframe. However, low wear values are evidence of lower stresses, but this assertion must be verified mathematically. This verification occurs in two steps.

Firstly, cycles to failure for eyebars in the finite life region of the S-N curve were normalized and plotted against wear, as shown in Figure 5-1. Cycles to failure required normalization to eliminate the effect of stress range on the relationship between wear and cycles. For low wear values on the curve, it can be seen that there is no correlation between wear and cycles to failure. However, cycles to failure appear to trend downward for the highest three wear values. Regardless, there is no clear trend between wear and cycles to failure by inspection of Figure 5-1 alone. It is prudent to seek out any possible relationships using other means besides Figure 5-1.

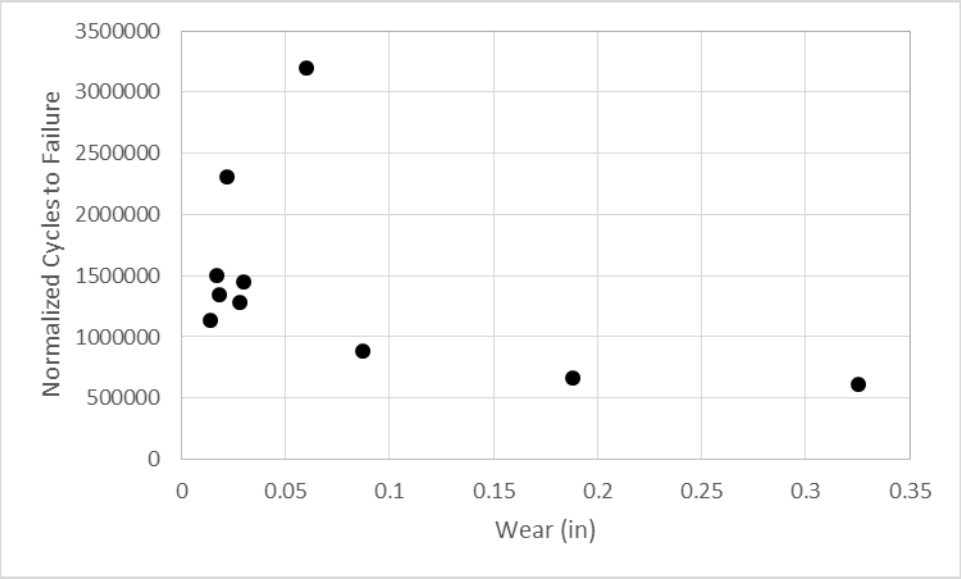

Figure 5-1 – Wear vs Normalized Cycles to Failure

Secondly, lasso regression was run on the eyebar wear data and a very small correlation was found between wear and fatigue life, that as wear increased, it had a small decreasing effect on cycle count. However, the relation is very weak. It is postulated that the reason that the wear values have only a small effect on the remaining useful life is that the stresses experienced by the eyebars were less than the fatigue threshold during their service lives. Stress histories less than the endurance limit would not leave residual fatigue damage due to their infinite life by definition. Therefore, it is expected that there is little or no predictive value for wear in eyebars that experienced stresses below the fatigue threshold. After optimization of the Lambda parameter of the Lasso correlation, the Beta values, which are the correlation coefficients showing the strength of the relationship, were -3.456 and -0.185 for stress range and wear respectively. This means that besides the correlation between wear and cycles to failure being very weak, stress range is 19 times more powerful in predictive value than wear is. We can conclude that probably very few eyebars in these bridges were subjected to stresses that exceeded the fatigue threshold during their service lives, however more data would be needed to increase the robustness of this inference. Even if most eyebars did not experience stress ranges above their fatigue thresholds, it is probable that some did, as the data suggest this is the case.

5.2 Inferences from Material Testing

From the material tests performed under this study, it can be concluded that the two bridges were constructed of two different steel types. It is evident that the Burlington Bridge material did not meet the specification prepared by its chief engineer

George Morison at the time of construction in 1893. The reason why this is the case is unclear, and troubling. It is troubling because the Burlington Bridge was in service for so long, having a material approximately 8 ksi below the specified design strength. The fact that there were no documented failures indicates the inherent conservativeness in the bridge design specification at the time.

5.3 Inferences from Fatigue Data

Inspection of fatigue data shows that from a fatigue design perspective, these eyebars would may not have met modern fatigue design requirements. This study has established with reasonable confidence that the eyebars mostly experienced stresses below 5.1 ksi, the current best estimate of the fatigue threshold for these eyebars. However, in Section 2.2, it was established that if the eyebars were to be designed today, they would be required to have a maximum stress range of 4.5 ksi from live load. Inspection of Figure 4-12 shows that in the finite life region, the results consistently fall below the fatigue curve for Category E, however the eyebars do show a threshold higher than the allowable. This threshold is independent of the stresses these eyebars are subjected to. Even though the evidence suggests that the stresses the eyebars experienced were below their fatigue thresholds, they could have still exceeded the design threshold as stipulated in AASHTO/AREMA.

5.4 Directions for Future Research

As noted earlier in this study, a finite element simulation would be the first additional research track taken to either confirm or deny the findings of this paper. Incorporation of wear stress models will also greatly enhance the conclusions of the

wear inferences. A meta-analysis of the statistical studies into bridge behavior could be performed to increase the robustness of the inferences drawn from the data in this study. Finally, more fatigue testing is needed in the finite life region of the S-N curve in order to further establish the fatigue behavior of these period bridges.

REFERENCES

AASHTO (2014). *AASHTO LRFD Bridge Design Specifications, U.S. Customary Units. 7th edition*, Washington, DC: American Association of State Highway and Transportation Officials, 7th edition.

Åkesson, B. (1994). "*Fatigue life of riveted railway bridges*." Dissertation, Chalmers University of Technology. Gothenberg, Sweden.

AREMA (2014). *Manual for Railway Engineering.* Landover, MD: American Railway Engineering and Maintenance-of-Way Association.

Bakht, B. and Jaeger, L. G. (1990). "*Bridge testing-a surprise every time*." Journal of Structural Engineering **116**(5): 1370-1383.

Basquin, O. (1910). "*The exponential law of endurance tests*." American Society of Testing Materials **10**(2): 625-630.

Bayoumi, M. R. and Abdellatif, A. K. (1995). "*Effect of surface finish on fatigue strength*." Engineering Fracture Mechanics **51**(5): 861-870.

Cooper, T. (1890). *General Specifications for Iron and Steel Railroad Bridges and Viaducts*. Engineering News Publishing Company. New York, New York.

DelGrego, M., Culmo, M. and DeWolf, J. (2008). "*Performance evaluation through field testing of century-old railroad truss bridge*." Journal of Bridge Engineering **13**(2): 132-138.

Fisher, J. W., Yen, B., Wang, D. and Mann, J. (1987). "*Fatigue and fracture evaluation for rating riveted bridges*." Transportation Research Board. NCHRP Report No. 302. Washington, DC.

Imam, B., Righiniotis, T. D. and Chryssanthopoulos, M. K. (2005). "*Fatigue assessment of riveted railway bridges*." Steel Structures **5**(5): 485-494.

Keating, P. and Fisher, J. W. (1986). "*Evaluation of fatigue tests and design criteria on welded details*." Transportation Research Board. NCHRP Report No. 286. Washington, DC

Kelton, S. L., Arwade, S. R. and Lutenegger, A. J. (2011). "*Variability of the mechanical properties of wrought iron from historic american truss bridges*." Journal of Materials in Civil Engineering **23**(5): 638-647.

Kirkaldy, D. (1862). *Results of an Experimental Inquiry into the Tensile Strength and other Properties of Various Kinds of Wrought-Iron and Steel*, Hamilton, Adams, and Co. London, England.

Kunz, F. (1915). *Design of Steel Bridges: Theory and Practice for the Use of Civil Engineers and Students*, McGraw-Hill Book Company, Incorporated. New York, New York.

Loveday, M. S., Gray, T. and Aegerter, J. (2004). "*Tensile testing of metallic materials: a review*." Final report of the TENSTAND project – Work Package 1. National Physical Laboratory. Teddington, UK.

Morison, G. S. (1893). "*Reconstruction of the burlington bridge*." Journal of the Association of Engineering Societies **12**: 599-614. Chicago, Illinois.

Nishanian, J. and Frank, K. H. (1972). "*Fatigue Characteristics of Steel Used in the Eyebars of the Point Pleasant Bridge*." U.S. Department of Transportation. Federal Highway Administration Report No. FHWA-RD-73-18.

Schijve, J. (2003). "*Fatigue of structures and materials in the 20th century and the state of the art*." International Journal of Fatigue **25**(8): 679-702.

Schijve, J. (2014). "*The significance of fatigue crack initiation for predictions of the fatigue limit of specimens and structures*." International Journal of Fatigue **61**: 39-45.

Schijve, J. (2009). *Fatigue of Structures and Materials*, Springer Science + Business Media, B.V. New York, New York.

Schütz, W. (1996). "*A history of fatigue*." Engineering Fracture Mechanics **54**(2): 263-300.

Sparks, S. (2008). "*Evaluation of iron and steel in historic bridges*." Structural Analysis of Historic Construction: Preserving Safety and Significance: Proceedings of the VI International Conference on Structural Analysis of Historic Construction: 451-458.

Waddell, J. A. L. (1916). *Bridge Engineering*, J. Wiley. New York, New York.

APPENDIX A

EYEBAR SUMMARY DATA AND TEST RESULTS

A.1 Eyebar Data

All force values are in kips, all dimensional values are in inches, and all stress values are in kips/in^2, ksi. Test specimens were taken from the locations designated by Configurations 1 and 2 below. Configuration 0 denotes no test specimens taken from an eyebar.

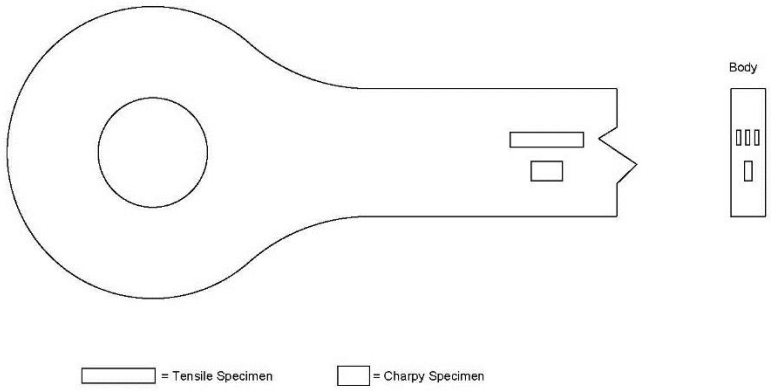

Figure A-1 - Test Specimen Locations: Configuration 1

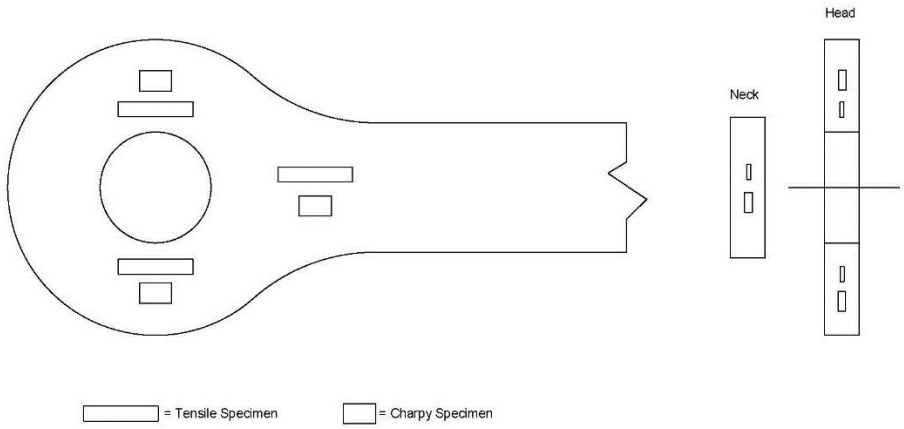

Figure A-2 - Test Specimen Locations: Configuration 2

Eyebar	**8-6?? (6B, Burlington, exact joint unknown)**
Test Designation	**FT-00**
Test Specimen Config.	1
Thickness (in)	N/A
Stress Range (ksi)	20
Fatigue Cycles to Failure	235175
Yield Strength (ksi)	30.703

Table A-1 – FT-00 Summary Data

Eyebar	**FT-01 (DS 47 East, Burlington)**
Test Specimen Configuration	1
Thickness, Width (in)	1.06, 16.563
Hole Diameter Longitudinal A (in)	6.013
Hole Diameter Transverse A (in)	5.989
Hole Diameter Longitudinal B (in)	6.031
Hole Diameter Transverse B (in)	6.027
Max Force (k)	175
Min Force (k)	70
Range (k)	105
Stress Range (ksi)	14.15
Fatigue Cycles to Failure	960,762
Estimated Hole Wear (in)	0.022

Table A-2 – FT-01 Summary Data

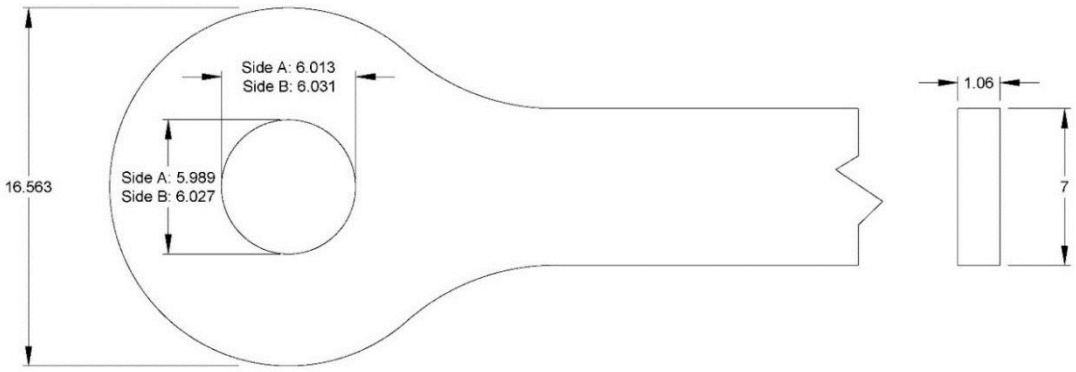

Figure A-3 – FT-01 Dimensions

Eyebar	**FT-02 (11-1, Oregon)**
Test Specimen Configuration	0
Thickness, Width (in)	1.928, 16.750
Hole Diameter Longitudinal A (in)	6.125
Hole Diameter Transverse A (in)	6.340
Hole Diameter Longitudinal B (in)	6.111
Hole Diameter Transverse B (in)	6.307
Max Force (k)	338
Min Force (k)	135
Range (k)	203
Stress Range (ksi)	15.04
Fatigue Cycles to Failure	224,861
Estimated Hole Wear (in)	0.325

Table A-3 – FT-02 Summary Data

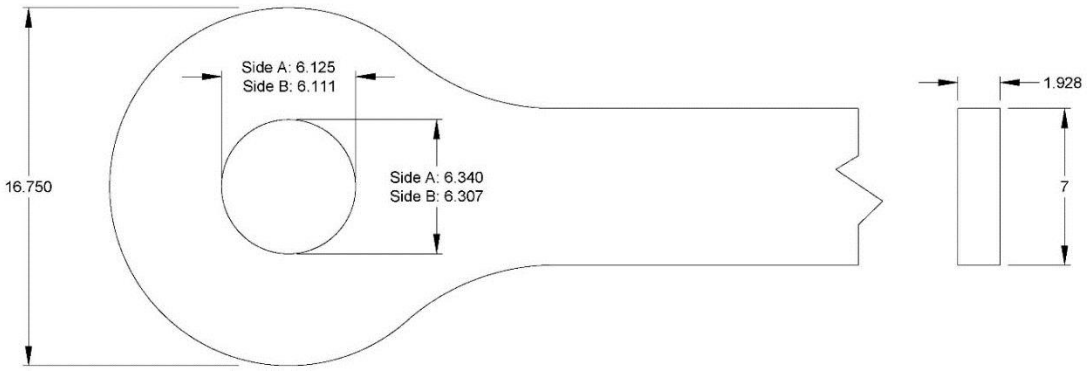

Figure A-4 – FT-02 Dimensions

Eyebar	**FT-03 (DS-47 East 1 Outside, Burlington)**
Test Specimen Configuration	0
Thickness (in)	1.055, 16.75
Hole Diameter Longitudinal A (in)	6.029
Hole Diameter Transverse A (in)	6.023
Hole Diameter Longitudinal B (in)	6.028
Hole Diameter Transverse B (in)	6.028
Max Force (k)	140
Min Force (k)	70
Range (k)	70
Stress Range (ksi)	9.48
Fatigue Cycles to Failure	1,656,031
Estimated Hole Wear (in)	0.014

Table A-4 – FT-03 Summary Data

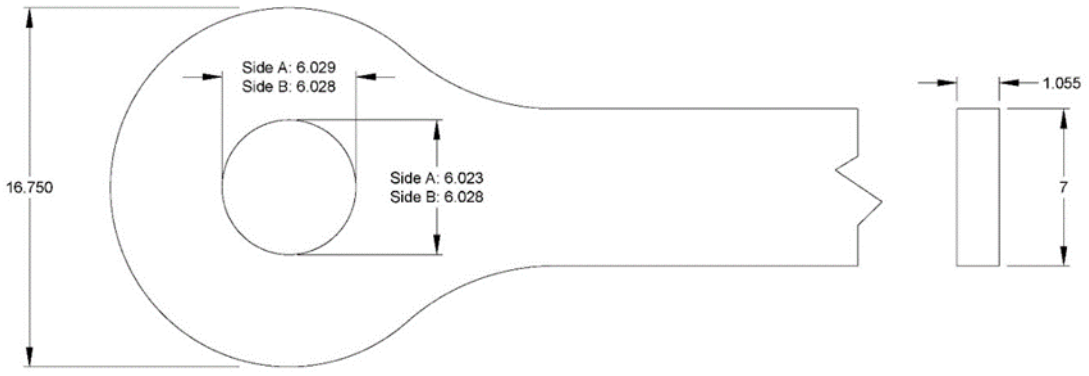

Figure A-5 – FT-03 Dimensions

Eyebar	**FT-04 (M/1-2, Burlington)**
Test Specimen Configuration	1
Thickness, Width (in)	1.284, 16.70
Hole Diameter Longitudinal A (in)	6.023
Hole Diameter Transverse A (in)	6.003
Hole Diameter Longitudinal B (in)	6.023
Hole Diameter Transverse B (in)	6.006
Max Force (k)	180
Min Force (k)	90
Range (k)	90
Stress Range (ksi)	10.01
Fatigue Cycles to Failure	1,826,938
Estimated Hole Wear (in)	0.017
Yield Strength (ksi)	27.297

Table A-5 – FT-04 Summary Data

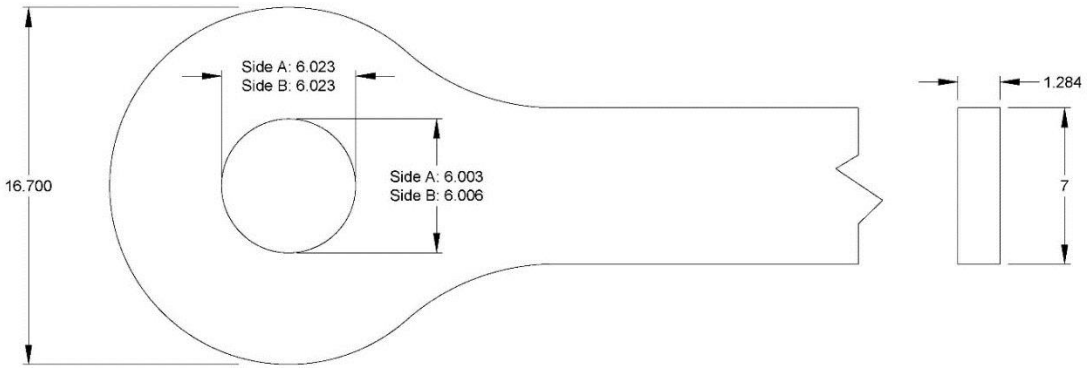

Figure A-6 – FT-04 Dimensions

Eyebar	**FT-05 (M/1-1, Burlington)**
Test Specimen Configuration	0
Thickness, Width (in)	1.268, 16.86
Hole Diameter Longitudinal A (in)	6.015
Hole Diameter Transverse A (in)	6.005
Hole Diameter Longitudinal B (in)	6.005
Hole Diameter Transverse B (in)	6.008
Max Force (k)	133
Min Force (k)	89
Range (k)	44
Stress Range (ksi)	4.96
Fatigue Cycles to Failure	12,000,000 (Runout)
Estimated Hole Wear (in)	0.012

Table A-6 – FT-05 Summary Data

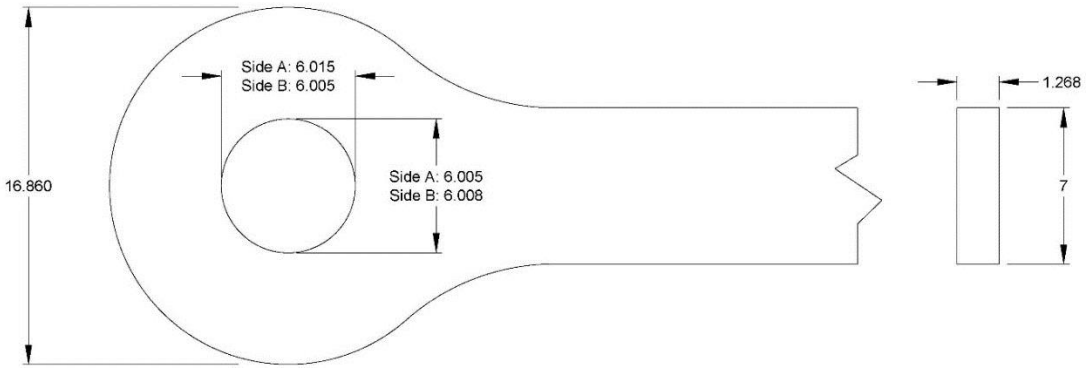

Figure A-7 – FT-05 Dimensions

Eyebar	**FT-06 (M/8-3, Burlington)**
Test Specimen Configuration	0
Thickness, Width (in)	1.260, 16.53
Hole Diameter Longitudinal A (in)	6.113
Hole Diameter Transverse A (in)	6.041
Hole Diameter Longitudinal B (in)	6.110
Hole Diameter Transverse B (in)	6.047
Max Force (k)	219
Min Force (k)	87.5
Range (k)	131.5
Stress Range (ksi)	14.91
Fatigue Cycles to Failure	311,153
Estimated Hole Wear (in)	0.087

Table A-7 – FT-06 Summary Data

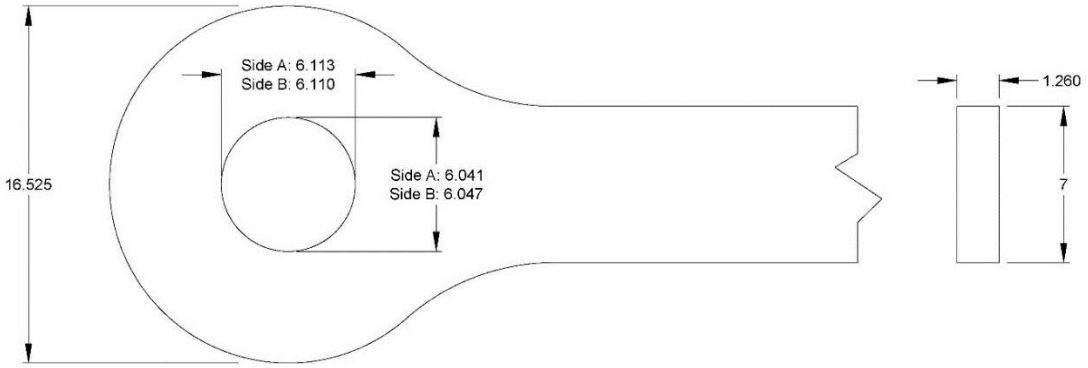

Figure A-8 – FT-06 Dimensions

Eyebar	**FT-07 (9-1, Oregon)**
Test Specimen Configuration	0
Thickness, Width (in)	1.945, 16.73
Hole Diameter Longitudinal A (in)	6.077
Hole Diameter Transverse A (in)	6.255
Hole Diameter Longitudinal B (in)	6.099
Hole Diameter Transverse B (in)	6.221
Max Force (k)	338
Min Force (k)	135
Range (k)	203
Stress Range (ksi)	14.91
Fatigue Cycles to Failure	248,061
Estimated Hole Wear (in)	0.188

Table A-8 – FT-07 Summary Data

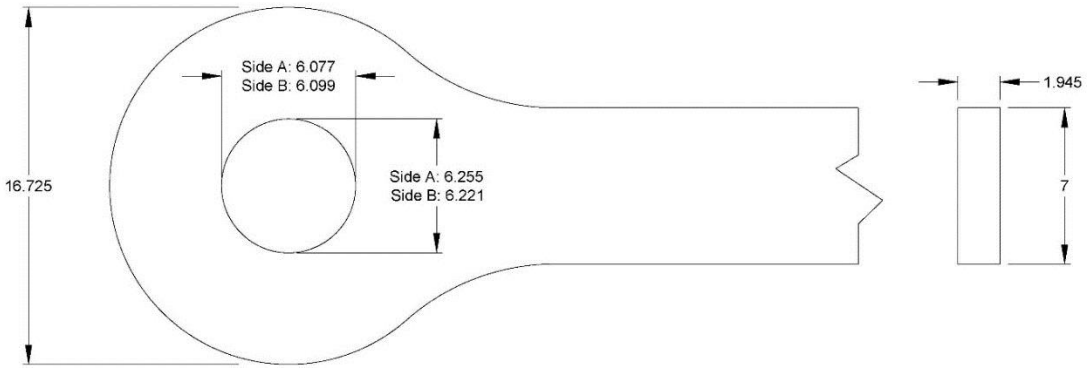

Figure A-9 – FT-07 Dimensions

Eyebar	**FT-08 (M/8-4, Burlington)**
Test Specimen Configuration	0
Thickness, Width (in)	1.296, 16.95
Hole Diameter Longitudinal A (in)	6.044
Hole Diameter Transverse A (in)	6.018
Hole Diameter Longitudinal B (in)	6.045
Hole Diameter Transverse B (in)	6.014
Max Force (k)	149
Min Force (k)	87.5
Range (k)	61.5
Stress Range (ksi)	6.78
Fatigue Cycles to Failure	13,302,022 (Runout)
Estimated Hole Wear (in)	0.034

Table A-9 – FT-08 Summary Data

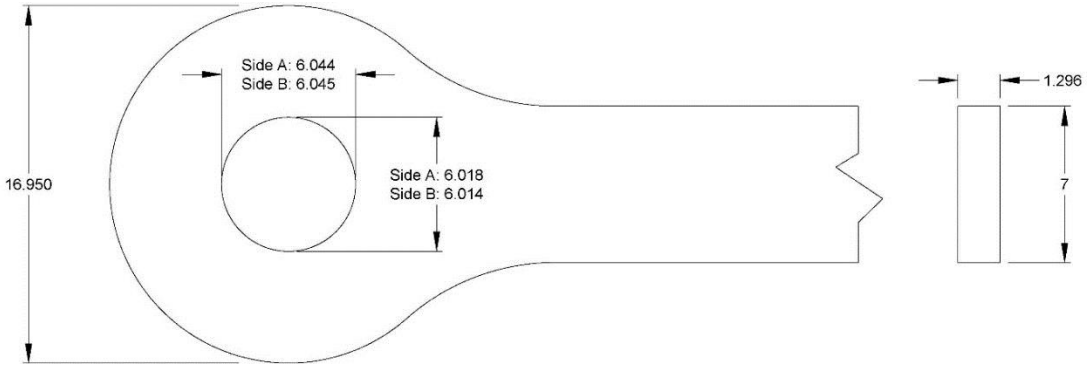

Figure A-10 – FT-08 Dimensions

Eyebar	**FT-09 (M/8-2, Burlington)**
Test Specimen Configuration	0
Thickness, Width (in)	1.259, 17.00
Hole Diameter Longitudinal A (in)	6.075
Hole Diameter Transverse A (in)	6.029
Hole Diameter Longitudinal B (in)	6.075
Hole Diameter Transverse B (in)	6.020
Max Force (k)	166
Min Force (k)	87.5
Range (k)	78.5
Stress Range (ksi)	8.907
Fatigue Cycles to Failure	6,012,200
Estimated Hole Wear (in)	0.060

Table A-10 – FT-09 Summary Data

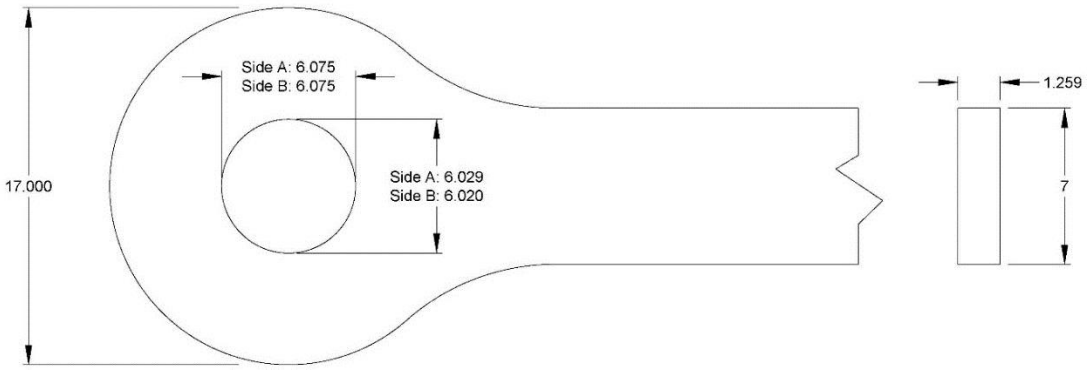

Figure A-11 – FT-09 Dimensions

Eyebar	**FT-10 (11-10, Oregon)**
Test Specimen Configuration	0
Thickness, Width (in)	1.94, 16.73
Hole Diameter Longitudinal A (in)	6.032
Hole Diameter Transverse A (in)	6.034
Hole Diameter Longitudinal B (in)	6.021
Hole Diameter Transverse B (in)	6.053
Max Force (k)	258
Min Force (k)	136
Range (k)	122
Stress Range (ksi)	8.984
Fatigue Cycles to Failure	2,190,320
Estimated Hole Wear (in)	0.028

Table A-11 – FT-10 Summary Data

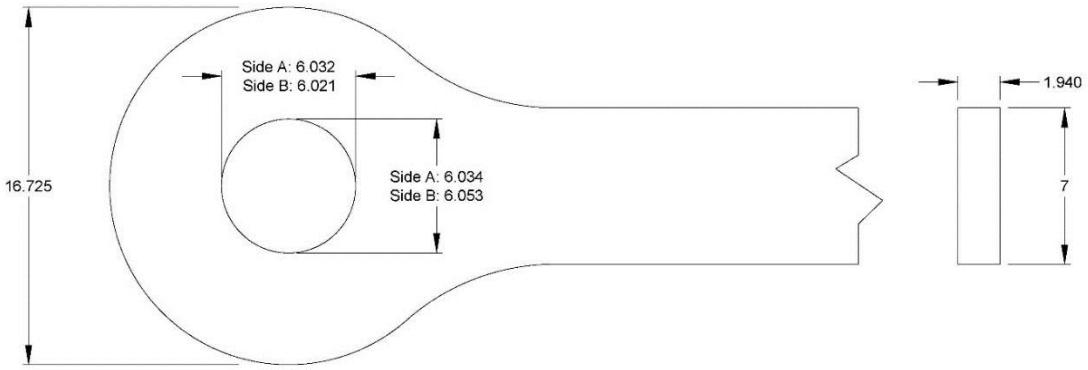

Figure A-12 – FT-10 Dimensions

Eyebar	**FT-11 (U8 D/S 6, Burlington)**
Test Specimen Configuration	0
Thickness, Width (in)	1.771, 16.44
Hole Diameter Longitudinal A (in)	6.028
Hole Diameter Transverse A (in)	6.023
Hole Diameter Longitudinal B (in)	6.003
Hole Diameter Transverse B (in)	5.988
Max Force (k)	233
Min Force (k)	123
Range (k)	110
Stress Range (ksi)	8.873
Fatigue Cycles to Failure	2,190,000
Estimated Hole Wear (in)	0.018

Table A-12 – FT-11 Summary Data

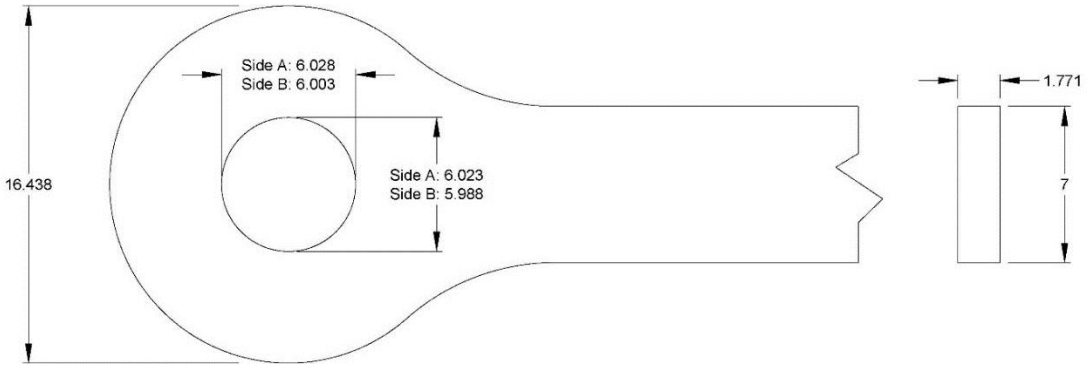

Figure A-13 – FT-11 Dimensions

Eyebar	**FT-12 (U8 U/S 6, Burlington)**
Test Specimen Configuration	0
Thickness, Width (in)	1.794, 16.63
Hole Diameter Longitudinal A (in)	6.001
Hole Diameter Transverse A (in)	6.006
Hole Diameter Longitudinal B (in)	6.027
Hole Diameter Transverse B (in)	6.018
Max Force (k)	221
Min Force (k)	123
Range (k)	98
Stress Range (ksi)	7.80
Fatigue Cycles to Failure	20,000,000 (Runout)
Estimated Hole Wear (in)	0.015

Table A-13 – FT-12 Summary Data

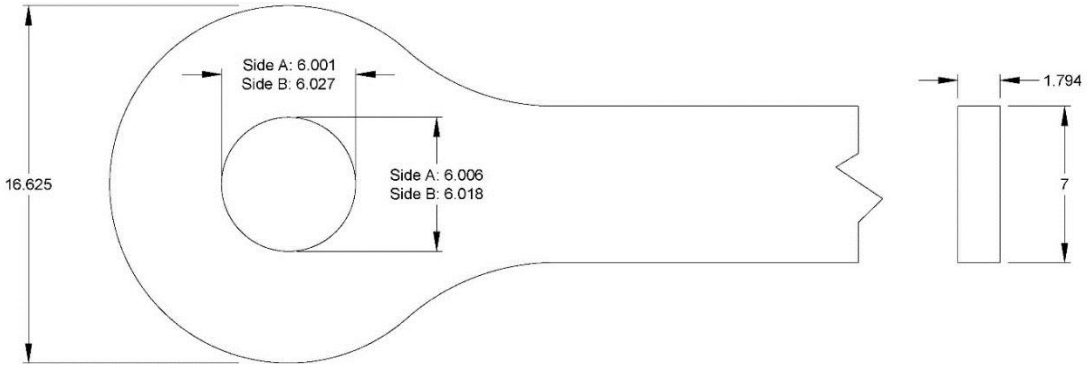

Figure A-14 – FT-12 Dimensions

A.2 Stress-Strain Curves for 11-7, 11-9

(11-7 and 11-9 were not fatigue tested.)

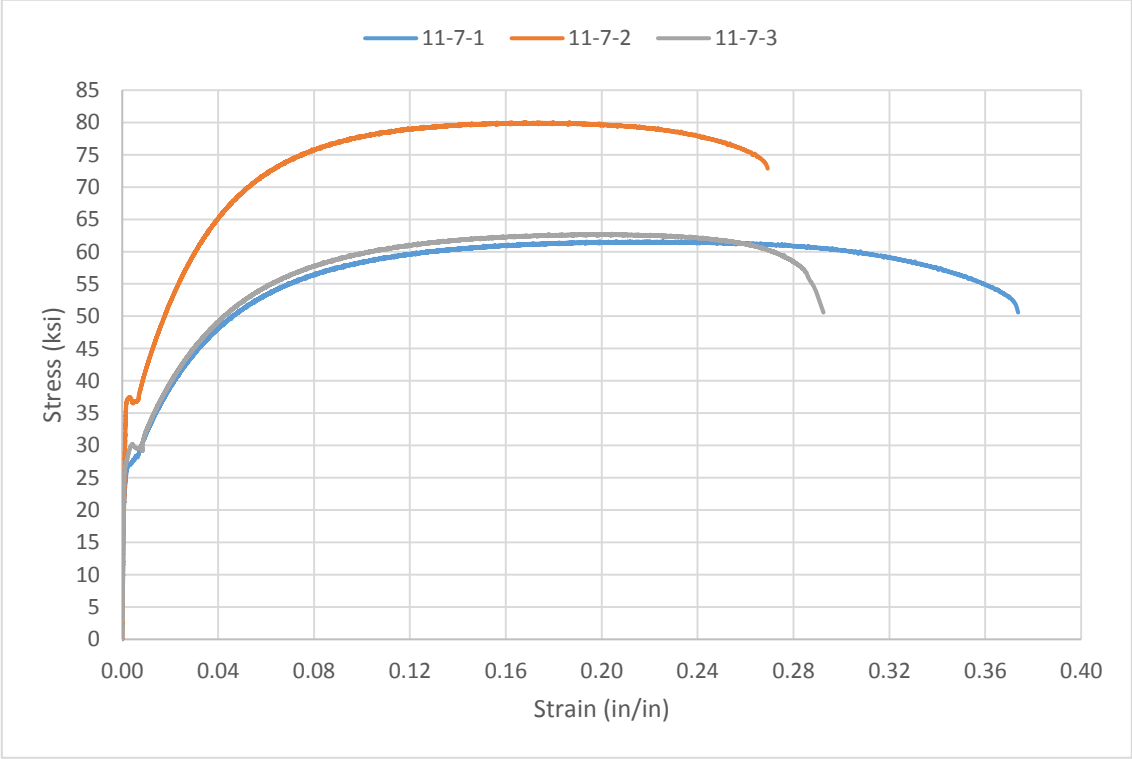

Figure A-15 – 11-7 Stress-Strain Curves

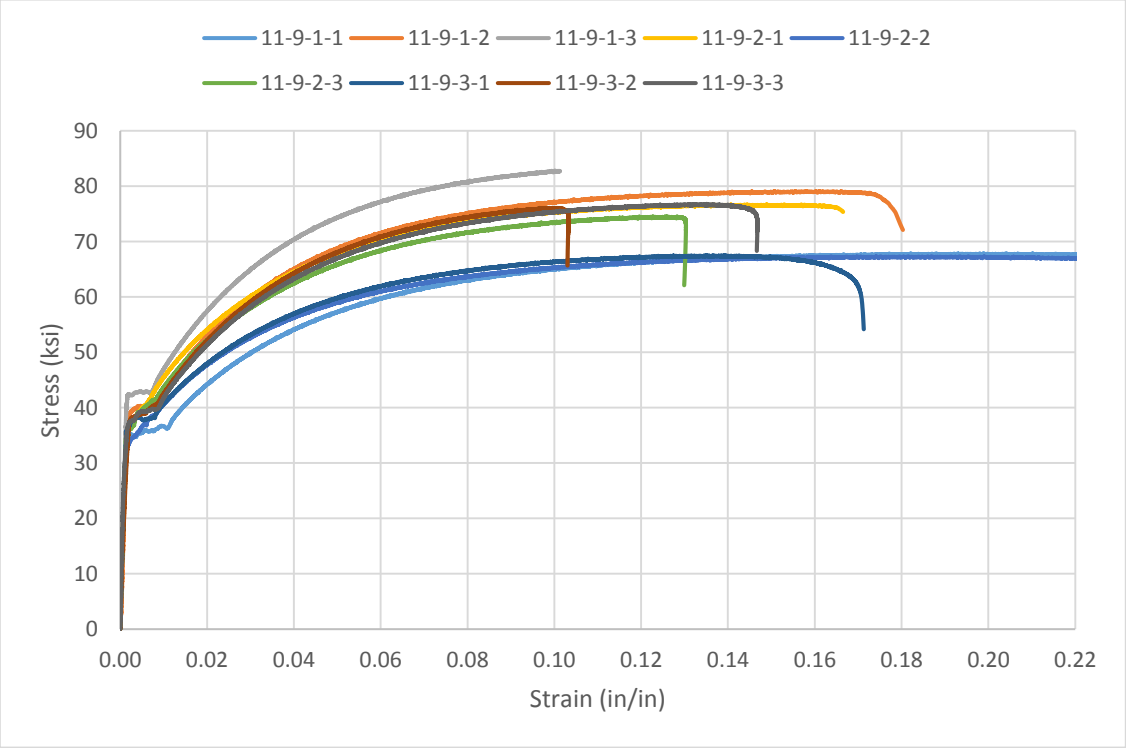

Figure A-16 – 11-9 Stress-Strain Curves

APPENDIX B

STATISTICAL TESTS

B.1 Eyebar Hole Diameter ANOVA Test

ANOVA Side A

SUMMARY

Groups	*Count*	*Sum*	*Average*	*Variance*
A Long.	32	194.215	6.069219	0.001639
A Trans.	32	194.314	6.072313	0.006185

ANOVA

Source of Variation	*SS*	*df*	*MS*	*F*	*P-value*	*F crit*
Between Groups	0.000153	1	0.000153	0.039143	0.843812	3.995887
Within Groups	0.242562	62	0.003912			
Total	0.242715	63				

ANOVA Side B

SUMMARY

Groups	*Count*	*Sum*	*Average*	*Variance*
A Long.	29	175.929	6.066517	0.001651
A Trans.	29	175.972	6.068	0.006291

ANOVA

Source of Variation	*SS*	*df*	*MS*	*F*	*P-value*	*F crit*
Between Groups	3.19E-05	1	3.19E-05	0.008028	0.928924	4.012973
Within Groups	0.222369	56	0.003971			
Total	0.222401	57				

Table B-1 – Eyebar Hole Diameter ANOVA Results

B.2 Bridge Tensile Yield ANOVA Test

ANOVA

SUMMARY

Groups	*Count*	*Sum*	*Average*	*Variance*
Burlington	12	364.3956	30.3663	7.738763
Oregon	12	437.0301	36.41917	19.1841

ANOVA

Source of Variation	*SS*	*df*	*MS*	*F*	*P-value*	*F crit*
Between Groups	219.8239	1	219.8239	16.3299	0.000546	4.30095
Within Groups	296.1515	22	13.46143			
Total	515.9754	23				

Table B-2: Bridge Yield Test ANOVA Results

APPENDIX C

MATLAB SCRIPTS

C.1 Material Data Analysis Script

```
%$ Material Data Analysis Script
%% Import data from spreadsheet for analysis
% Script for importing data from the following spreadsheet:
%
%    Workbook: C:\Users\CAB\Google Drive\Research\Fatigue Project\Test
Data\Summary Data.xlsx
% Auto-generated by MATLAB on 2016/08/12 17:50:07

%% Import the data
[~, ~, raw] = xlsread('C:\Users\CAB\Google Drive\Research\Fatigue
Project\Test Data\Summary Data.xlsx','Summary','B30:G41');

%% Create output variable
data = reshape([raw(AASHTO)],size(raw));

%% Allocate imported array to column variable names
BurlingtonUlt = data(:,1);
OregonUlt = data(:,2);
BurlingtonYield = data(:,3);
OregonYield = data(:,4);
BurlingtonT = data(:,5);
OregonT = data(:,6);
clearvars data raw;
%%
[~, ~, raw] = xlsread('C:\Users\CAB\Google Drive\Research\Fatigue
Project\Test Data\Summary Data.xlsx','Summary','D2:F25');
data = reshape([raw{:}],size(raw));
E_vals = data(:,1);
Elong = data(:,2);
toughness = data(:,3);
clearvars data raw;

Yields = [BurlingtonYield; OregonYield];
Ults = [BurlingtonUlt; OregonUlt];
T = [BurlingtonT; OregonT];
predictors = [Yields Ults E_vals Elong];

%% Fit distribution
pd = fitdist(BurlingtonYield,'Normal')
paramci(pd,'Alpha',.05)
[hnorm,pnorm,adstat,cv] = adtest(Yields)
x = 20:.1:40;
y = pdf(pd,x);
```

```
%% Whitney-Mann test on difference between bridge yields and ultimate
values
p = ranksum(BurlingtonYield,OregonYield)
[h1,pt1] = ttest2(BurlingtonYield,OregonYield,'Vartype','unequal')
[h2,pt2] = ttest2(BurlingtonUlt,OregonUlt,'Vartype','unequal')
[h3,pt3] = ttest2(BurlingtonT,OregonT,'Vartype','unequal')

%% Plots
figure(1)
subplot(2,1,1)
boxplot(BurlingtonYield)
ylabel('Yield Stress (ksi)')
xlabel('Quantiles')
title('Burlington Bridge Yield (n=12)')
subplot(2,1,2)
boxplot(OregonYield)
ylabel('Yield Stress (ksi)')
xlabel('Quantiles')
title('Oregon Bridge Yield (n=12)')
figure(2)
plot(x,y)
```

C.2 Lasso Regression Script

```
%% Import data from spreadsheet
% Script for importing data from the following spreadsheet:
%
%    Workbook: C:\Users\CAB\Google Drive\Research\Fatigue
Project\Eyebar Fatigue Cycles.xlsx
%    Worksheet: Sheet1
% Auto-generated by MATLAB on 2016/09/23 15:15:28

%% Import the data
[~, ~, raw] = xlsread('C:\Users\CAB\Google Drive\Research\Fatigue
Project\Eyebar Fatigue Cycles.xlsx','Sheet1','D2:F13');

%% Create output variable
data = reshape([raw{:}],size(raw));

%% Allocate imported array to column variable names
StressRange = log(data(:,1));
WearPrime = data(:,2);
Wear = log(data(:,2));
CyclesPrime = data(:,3)
Cycles = log(data(:,3));
scatter3(StressRange,Wear,Cycles)
%% Clear temporary variables
clearvars data raw;

%%Run Lasso Regression
predictors = [StressRange Wear];
[B,FitInfo] = lasso(predictors,Cycles,'CV',3)
```

```
lassoPlot(B,FitInfo,'PlotType','CV')
FitInfo.Lambda(FitInfo.IndexMinMSE)
B(1,FitInfo.IndexMinMSE)
B(2,FitInfo.IndexMinMSE)
```

C.3 Distribution Fitting Script

```
clear
clc
%%%Test pdfs against wear data distribution

%% Import the data
[~, ~, raw] = xlsread('C:\Users\CAB\Google Drive\Research\Fatigue
Project\Eyebar Inventory and Summary_Master.xlsx','Sheet1','K2:K71');

%% Create output variable
wear = reshape([raw{:}],size(raw));

%% Clear temporary variables and and remove NaN from wear variable
clearvars raw;
wear(isnan(wear)) = [];

%Histogram of Wear Data
[nelements,centers] = hist(wear);
xlabel('Wear (in)');
ylabel('Frequency');
title('Eyebar Wear Data Histogram')
wearchidata = [centers' nelements'];

%Fit Distribution to Data
pd1 = fitdist(wear,'Weibull')
pd2 = fitdist(wear,'Lognormal')
pd3 = fitdist(wear,'exp')
x_values = 0:0.001:0.4;
fit1 = pdf(pd1,x_values);
fit2 = pdf(pd2,x_values);
fit3 = pdf(pd3,x_values);
figure(1)
hist(wear,12)
hold on
plot(x_values,fit1,'c',x_values,fit2,'m',x_values,fit3,'r')
legend('Histogram','Weibull','Lognormal','Exponential')
title('Distribution Fit for Wear
Data','FontSize',12,'FontWeight','bold')
ylim([0,12])

%Perform Anderson Darling Goodness of Fit test
[hweib,pweib,statweib] = adtest(wear,'Distribution','Weibull');
[hlog,plog,statlog] = adtest(wear,'Distribution','Lognormal');
[hexp,pexp,statexp] = adtest(wear,'Distribution','exp');

%Output stats in table form
```

```
pvalues = [pweib plog pexp];
stats = [statweib statlog statexp];
output = cell(4,1);
output{1,1} = {'Distribution' 'P Value' 'AD Stat.'};
output{2,1} = {'Weibull' pweib statweib};
output{3,1} = {'Lognormal' plog statlog};
output{4,1} = {'Exponential' pexp statexp};
reshape([output{:}]',[],length(output))
figure(2)
probplot('lognormal',wear)
figure(3)
probplot('exponential',wear)
figure(4)
plot(x_values,cdf(pd1,x_values))
hold on
ecdf(fit1)
```